Spatial and temporal monitoring of soil water content with an irrigated corn crop cover using surface electrical resistivity tomography

Didier Michot, Yves Benderitter, Abel Dorigny, Bernard Nicoullaud, Dominique King, Alain Tabbagh

Spatial and temporal monitoring of soil water content with an irrigated corn crop cover using surface electrical resistivity tomography

Didier Michot,[1] Yves Benderitter,[2] Abel Dorigny,[1] Bernard Nicoullaud,[1] Dominique King,[1] and Alain Tabbagh[2]

Received 15 July 2002; revised 13 November 2002; accepted 18 February 2003; published 27 May 2003.

[1] A nondestructive and spatially integrated multielectrode method for measuring soil electrical resistivity was tested in the Beauce region of France during a period of corn crop irrigation to monitor soil water flow over time and in two-dimensional (2-D) with simultaneous measurements of soil moisture and thermal profiles. The results suggested the potential of surface electrical resistivity tomography (ERT) for improving soil science and agronomy studies. The method was able to produce a 2-D delimitation of soil horizons as well as to monitor soil water movement. Soil drainage through water uptake by the roots, the progression of the infiltration front with preferential flow zones, and the drainage of the plowed horizon were well identified. At the studied stage of corn development (3 months) the soil zones where infiltration and drainage occurred were mainly located under the corn rows. The structural soil characteristics resulting from agricultural practices or the passage of agricultural equipment were also shown. Two-dimensional sections of soil moisture content were calculated using ERT. The estimates were made by using independently established "in situ" calibration relationships between the moisture and electrical resistivity of typical soil horizons. The thermal soil profile was also considered in the modeling. The results showed a reliable linear relationship between the calculated and measured water contents in the crop horizon. The precision of the calculation of the specific soil water content, quantified by the root mean square error (RMSE), was 3.63% with a bias corresponding to an overestimation of 1.45%. The analysis and monitoring of the spatial variability of the soil moisture content with ERT represent two components of a significant tool for better management of soil water reserves and rational irrigation practices. *INDEX TERMS:* 0925 Exploration Geophysics: Magnetic and electrical methods; 1866 Hydrology: Soil moisture; 1875 Hydrology: Unsaturated zone; 5109 Physical Properties of Rocks: Magnetic and electrical properties; *KEYWORDS:* soil moisture, unsaturated soil, electrical resistivity tomography, monitoring, infiltration, drying

Citation: Michot, D., Y. Benderitter, A. Dorigny, B. Nicoullaud, D. King, and A. Tabbagh, Spatial and temporal monitoring of soil water content with an irrigated corn crop cover using surface electrical resistivity tomography, *Water Resour. Res.*, *39*(5), 1138, doi:10.1029/2002WR001581, 2003.

1. Introduction

[2] To provide an adequate water supply for growing corn, one must obtain precise knowledge of the soil moisture state. It is necessary to monitor water content changes in the field to measure water losses through infiltration and evapotranspiration. Better knowledge of soil water flow also gives a better understanding of the behavior and transport of agricultural pollutants. In consequence, a rational sampling strategy can be established to study the active time of the molecules residence.

[3] As soil electrical resistivity is related to its water content, the general aim of this study is to determine soil moisture with electrical resistivity, or more specifically to relate soil electrical resistivity changes with water content changes in an unsaturated soil.

[4] The first step of this study is to verify the capacity of the multielectrode method to monitor over time the soil water dynamics under an irrigated corn crop (Zea mays L.), particularly water infiltration and soil drainage by root uptake. The second step is to obtain 2-D soil water content sections after calibration of the electrical resistivity of typical soil horizons according to their moisture. The third step is to test the calculated water content with regard to soil water content measured simultaneously with electrical resistivity.

[1] Institut National de la Recherche Agronomique Orléans, Unité de Science du Sol, Olivet, France.
[2] UMR 7619 "Sisyphe", UMPC, CNRS, case 105, Paris, France.

0043-1397/03/2002WR001581

2. Review of Soil Water Content Measurements

2.1. Standard Measurements

[5] In addition to direct weighing method, soil water and moisture profiles can be obtained with numerous indirect methods where sensors are placed in the soil at different

depths. The neutron probe [*Gardner and Kirkam*, 1952; *Bavel et al.*, 1956] is a reliable water content measurement method [*Chanasyk and Naeth*, 1996], but its use is limited because radioactive source produces numerous constraints. Measurements of dielectric soil properties by TDR (time domain reflectometry) probes [*Topp et al.*, 1980] or capacitance sensors [*Bell et al.*, 1987; *Dean et al.*, 1987] avoid the use of radioactive sources. Time domain reflectometry is a technique to estimate the volumetric soil water content. It is based on the determination of the apparent dielectric constant K of soil. This quantity is calculated from the velocity of propagation of an electromagnetic signal in the frequency range of 1 MHz to 1 GHz along a transmission line in the soil, neglecting losses along the line as reviewed by *Topp and Davis* [1985]. Soil volumetric water content θ is calculated using an empirical relationship, which is independent of soil type, soil density, soil temperature and soluble salt content [*Topp et al.*, 1980]:

$$\theta = -5.3 \times 10^{-2} + 2.92 \times 10^{-2}\mathrm{K} - 5.5 \times 10^{-4}\mathrm{K}^2 + 4.3 \times 10^{-6}\mathrm{K}^3 \quad (1)$$

The precision of volumetric water content measurement is about ±2%. The water potential, which must be known to understand water flow in an unsaturated soil, is measured with a tensiometer. Water infiltration into the soil is not uniform. The vertical and horizontal soil water content is highly variable and depends on preferential flow directions [*Kung.*, 1990a, 1990b; *Herkelrath et al.*, 1991; *Ritsema et al.*, 1993; *Ritsema and Dekker*, 1994; *Flury et al.*, 1994]. Soil moisture sensors yield only restricted information and are often not representative of the spatial soil water distribution. Now, improved measurement techniques and automated methods, such as multiTDR systems have made possible soil moisture changes monitoring over time at different locations and detection of preferential water flow directions [*Heimovaara and Boulten*, 1990; *Herkelrath et al.*, 1991]. Still, these systems offer information at only a series of point locations rather than continuously at the field scale. Moreover, inserting moisture sensors disturbs the soil structure and the water flow [*Rothe et al.*, 1997].

[6] Many alternative methods have been tested in order to monitor water flow within the soil over time. Soluble dye tracers added to soil water have been used [*Kung*, 1990a, 1990b; *Flury et al.*, 1994; *Scanlon and Goldsmith*, 1997]. With this method, the spatial distribution of the dye tracer in the soil can be observed and therefore the infiltration zone can be determined. As a soil pit must be dug at the experimental site to monitor tracer infiltration, the soil structure is disturbed and the obtained information may not be representative of the actual processes under investigation. For example, the water flow may be perturbed by the changed soil drainage induced when a soil pit is dug.

[7] Nevertheless, it is difficult to obtain a 2-D or 3-D representation of the water flow in the soil by exploiting sparse local data. Geophysical surface methods are not intrusive and consequently do not disturb the soil structure. Also, each measurement integrates a greater volume of soil. These methods represent alternative ways of monitoring unsaturated soil water fluxes. The following discussion focuses on the use of ERT to monitor moisture changes in soil over time.

2.2. Use of Surface Geophysical Methods for Estimating Water Content and Infiltration

[8] Various surface geophysical methods have been used by hydrogeologists and soil scientists to identify soil water infiltration and water flow. In the past, much research has been performed using ground penetrating radar (GPR) to detect buried objects, to delineate geological structures and to measure the soil water content [*Davis and Annan*, 1989; *Hubbard et al.*, 1997; *Eppstein and Dougherty*, 1998; *Weiler et al.*, 1998; *Parkin et al.*, 2000]. The majority of the studies have produced positive results. *Daily and Ramirez* [1989] tested dielectric permittivity using borehole electromagnetic tomography to map water content changes in a heated volcanic ignimbrite. *Weiler et al.* [1998] concluded that in comparison with TDR measurements, GPR gave promising results for nondestructive water content measurements. *Hubbard et al.* [1997] showed that the joint use of GPR and conventional borehole data improves water saturation estimates for geological formations. By comparing radar wave velocity before and after a controlled release of salt water in the vadose zone, *Eppstein and Dougherty* [1998] detected and visualized soil moisture patterns in three dimensions. Recently, *Parkin et al.* [2000] showed the ad-vantage of GPR in monitoring soil water content distribution in a horizontal plane located below a wastewater trench. *Hubbard et al.* [2002] and *Huisman et al.* [2001] showed how GPR ground wave data could be used effectively to map near surface changes in water content. GPR performance is optimal in a soil with a coarse texture, but the performance decreases in electrically conductive media such as clayey soils.

[9] The nuclear magnetic resonance (NMR) method uses the nuclear properties of hydrogen to assess water content. In the ground, most hydrogen atoms are found in the water molecules. The NMR method can detect water directly, whereas conventional geophysical methods provide only indirect knowledge of soil moisture. Using NMR, the water content distribution and ground porosity versus depth have been estimated [*Amin et al.*, 1993; *Goldman et al.*, 1994; *Beauce et al.*, 1996]. However, NMR measurements are not suitable for superficial soil studies, as the first few meters below the land surface constitute a blind zone for that method.

[10] Soil electrical resistivity is a function of the textural and structural characteristics and is particularly sensitive to its water content [*Sheets and Hendrickx*, 1995]. Soils are a porous medium, made of nonconductive solid particles and containing electrolytes solution that can conduct electric current by the movement of the free ions in the bulk solution and ions adsorbed at the matrix surface. Precipitation and seasonal variations in soil temperature and soil water content cause significant changes in the electrical resistivity of the soil [*Aaltonen*, 1997; *Benderitter and Schott*, 1999]. Water infiltration and aquifer recharge can be detected by studies of variations in electrical sounding curves [*Barraud et al.*, 1979; *Cosentino et al.*, 1979]. Groundwater flow direction and velocity can be determined through observation of the electrical resistivity decrease in alluvial deposits following salt water tracer injections [*White*, 1994]. Recent development of a surface multielectrode method, known as electrical resistivity tomography (ERT), offers some interesting perspectives. This method is particularly well suited to the 2-D description

Figure 1. Location of the study area.

of geological structures perpendicular to the measurement electrode line [*Griffiths and Turnbull*, 1985; *Griffiths et al.*, 1990; *Shima*, 1990; *Griffiths and Barker*, 1993]. ERT presents great advantages for monitoring and is used in hydrological and environmental studies to monitor solutes and fluid flow in porous media. Monitoring of vadose zone water flow such as water infiltration, root water uptake, borehole pumping test effects has been reported by many authors [*Barker and Moore*, 1998; *Benderitter and Schott*, 1999; *Binley et al.*, 2001]. *Hagrey and Michaelsen* [1999], and *Michot et al.* [2001] adapted the electrode set up to reach a finer resolution in order to monitor soil water infiltration in 2-D. Recent progress in modeling and geo-physical 3-D inversion methods greatly reduced calculation errors and processing time [*Zhang et al.*, 1995]. Three-dimensional monitoring of small fresh water plume movements through the vadose zone has become possible [*Park*, 1998]. *Zhou et al.* [2001] also proposed a noninvasive me-thod to monitor, in the field, soil water content changes over time by means of 3-D electrical tomography. The cited works revealed the capability of ERT data in monitoring water infiltration in unsaturated soil or through the vadose zone, as is our focus. However, these works did not consider the possibility of obtaining a water content cross section from ERT data using a field-scale calibration method and taking into account the soil thermal profile. This current study, unlike the previous ones, investigates water flow dynamics in relation to the soil management (agricultural prac-tices, tillage operations) with a corn crop cover irrigated by sprinkling.

3. Presentation of the Study Site

[11] The study area is located southwest of Paris, in the Beauce region, at Villamblain (Figure 1). The topography is weakly undulating with slopes rarely exceeding 2%. The altitude ranges between 121 m and 125 m. The loamy clay soil has a thickness of 0.3 to 1.2 m over the Beauce limestone bedrock, containing a large aquifer about between 15 and 70 m depth. The water is pumped for crop irrigation and regional drinking water supply.

[12] The studied site has a corn crop cover (Zea mays L) and is irrigated by sprinklers. The experimental plot soil can be classified as a loamy clay Calcisol developed in a beige cryoturbated limestone deposit according to the French soil reference system [*Baize and Girard*, 1995]. Because of numerous studies about the regional spatial soil distribution and the experimental plot [*Isambert and Duval*, 1992; *Nicoullaud et al.*, 1997], this Calcisol was chosen as representative of the soil in the region. A soil pit was dug near the experimental device to identify the characteristic soil horizons (Figure 2). Three reference horizons include the following: (1) First is the top horizon, LAci, an organomineral 30 cm thick plow layer. It has a loamy clay texture, a fine polyhedral structure and a very high porosity. A plowed pan lies beneath its lower boundary. (2) Second is a light brown structural S horizon with slight weathering, observed at a depth from 30 cm to 75 cm. It is a loamy clay layer without coarse fragments and with a medium polyhedral structure and high porosity. This horizon is subdivided into three parts: Sci_1, Sci_2 and Sca_3. This division is justified by a decrease in clay content, a gradual weakening of soil structure and an increase of carbonate inflorescences inside earthworm burrows with depth. (3) Third is the Ck horizon at a 75 cm depth. It is formed of beige cryoturbated and highly weathered soft limestone rocks. It has a massive structure and a high porosity. This horizon is subdivided into two layers, $Ck(m)_1$ (75–100 cm) and Ck_2 (100–170 cm). On the basis of simultaneous decrease of clay and silt content and increase of carbonate content ($CaCO_3 > 75\%$) with depth.

[13] An auger drilling into the bottom of the soil pit provides additional information at depth. The Ck_2 horizon goes down to a depth of 170 cm. A soft powdery gray limestone mineral horizon Ck_3 exists between 170 and 250 cm depth. Beyond this, the auger was blocked by a slab of sublithographic hard gray Beauce Limestone. Table 1 shows particle size distribution of the fine earth fraction after carbonate removal and chemical analysis. The soil is alkaline (pH > 8.2). There is slight recarbonatation of the LAci surface horizon with regard to horizon Sci_1, no doubt related to the working of the soil and the use of irrigation water rich in calcium carbonate. The exchange complex is saturated with calcium throughout the soil profile.

[14] The corn crop was sown on 21 April 2000 with a density of 90,000 pl/ha and a distance of 0.80 m between rows. The soil was plowed to a depth of 30 cm and reworked on the surface by a harrow to reduce the size of the superficial clumps. The corn root profile (on the left of Figure 2) shows that the corn root density is higher in the plowed horizon between a depth of 0.1 and 0.3 m. The corn root density decreases rapidly with depth [*Nicoullaud et al.*, 1995]. This is a representative and typical soil of the Beauce region, which covers 85000 ha. Major soil differences are associated with only the thickness of the loamy-clay horizon and the $CaCO_3$ content.

4. Field Calibration

[15] A considerable effort has gone toward investigating the relationship between the apparent electrical resistivity

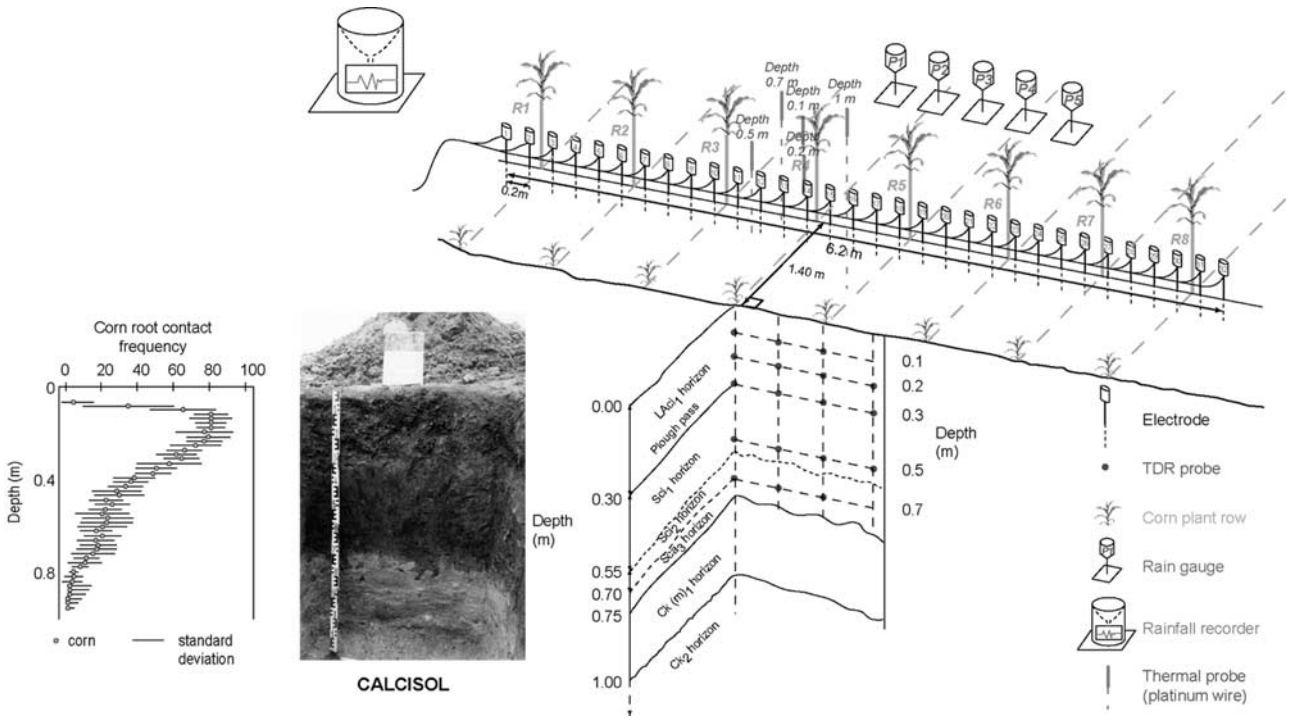

Figure 2. Water flow monitoring; experimental setup by 2-D electrical resistivity tomography in its pedological and agricultural context.

(or its reciprocal, the apparent electrical conductivity), water conductivity and water content in saturated and unsaturated porous media. Numerous reviews of these petrophysical models have been published [*Bussian*, 1983; *Worthington*, 1985; *Mualem and Friedman*, 1991; *Benderitter and Schott*, 1999] and their respective advantages and drawbacks have been discussed. The first model was established for clean sand, i.e. without any clay, in saturated or unsaturated conditions [*Archie*, 1942]. This model can not be used for the soil at our study site, which is a much more heterogeneous soil that contains clays. *Wyllie and Southwick* [1954] suggested that an aggregate of conductive particles saturated with a conductive electrolyte could be modeled with a three resistor network. *Waxman and Smits* [1968] proposed the first extensive model of shaly sand formations. They proposed that clay particles contribute exchange cations to the electrolyte thereby increasing the conductivity of the formation. The dual water model suggested by *Clavier et al.* [1977] is based on the assumption that the exchange cations contribute to the conductivity of a clay water which is spatially separated from the bulk water located in the pore space. More complex theoretical relationship were proposed relying upon properties of a solid phase dispersed in a continuous electrolyte [*Bussian*, 1983] or accounting for the different behavior of ions in the spore space [*Revil et al.*, 1998]. *Mualem and Friedman* [1991] proposed a model more adapted for soil at any water saturation but it does not take into account the surface conductivity. So, in unsaturated condition this model seems more adapted for soil with a coarse texture. The quality of the prediction decreases for fine texture as clayed soil. Most published models are either theoretical and present some physical limits, or are obtained in laboratory on small soil cores with controlled conditions.

[16] We considered the use of both laboratory-derived and field-derived petrophysical relationships for application to our field-scale ERT data. We attempted to use a laboratory calibration because it was easier and faster to measure the soil core electrical resistivity on a vast range of soil moisture. During a drying period, electrical resistivity and water content were measured on a cylindrical soil core from LAci and Sci_1 loamy-clay horizons. As expected, a high soil electrical resistivity decrease was observed as soil volumetric water content increased up to 15%, and when the soil volumetric

Table 1. Physical and Chemical Analyses of a Calcisol[a]

Horizon	Depth, cm	C, %	FS, %	CS, %	Fsa, %	Csa, %	$CaCO_3$, %	pH	CEC, cmol kg^{-1}	Ca^{++}, cmol kg^{-1}	Na^{+}, cmol kg^{-1}	Mg^{++}, cmol kg^{-1}	K^{+}, cmol kg^{-1}	da
LAci	0–30	32.0	29.2	32.3	2.1	0.4	4.0	8.2	20.3	43.6	0.082	1.12	0.766	1.27
Sci_1	30–55	32.3	30.4	34.1	1.7	0.2	1.3	8.3	18.0	32.7	0.084	0.83	0.422	1.45
Sci_2	55–70	29.4	30.1	34.3	1.5	0.1	4.6	8.4	14.4	45.9	0.103	0.64	0.287	-
Sca_3	70–75	17.1	20.8	24.0	1.1	0.2	36.8	8.6	9.2	44.3	0.078	0.43	0.168	-
$Ck(m)_1$	75–100	13.4	14.4	16.4	1	0.5	54.3	-	-	-	-	-	-	1.51
Ck_2	100–120	8.0	4.5	7.5	1.8	0.8	77.4	-	-	-	-	-	-	-

[a]Particle size analyses following carbonate removal. C, clay; FS, fine silt; CS, coarse silt; FSa: fine sand; CSa: coarse sand (X31-107); da: bulk density.

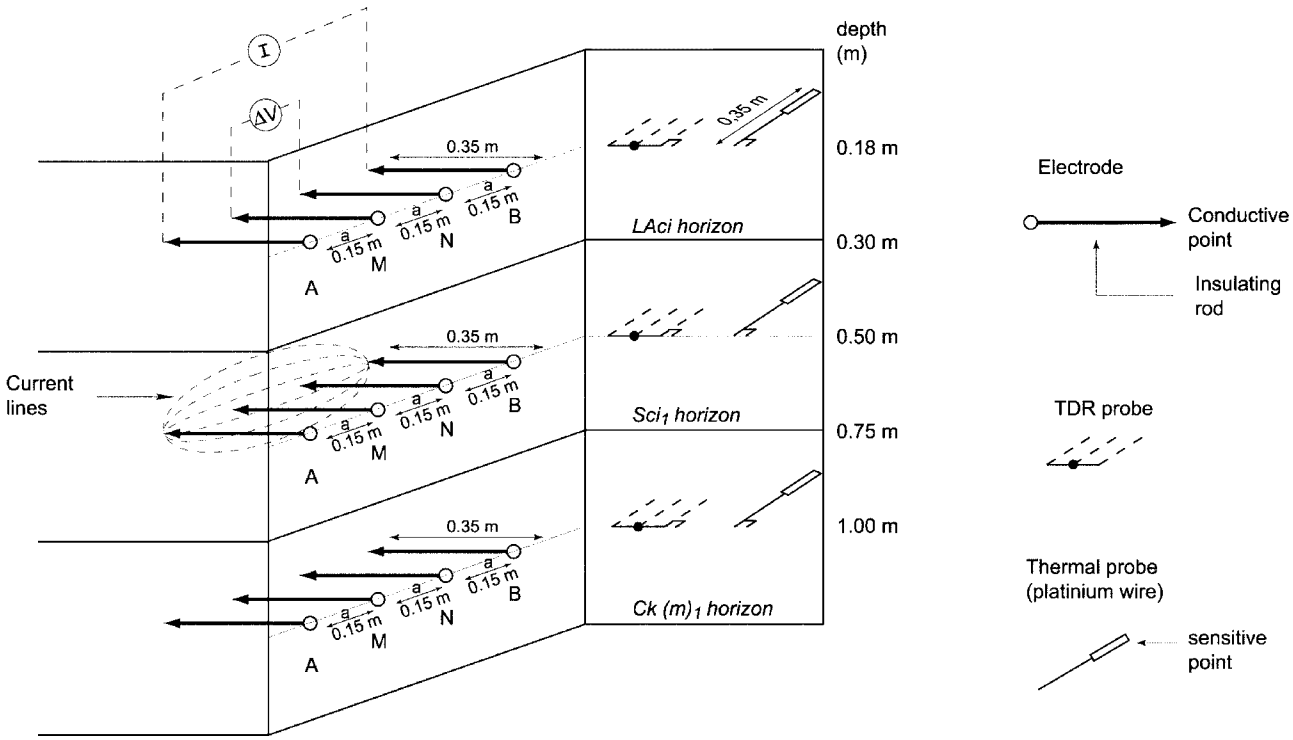

Figure 3. Experimental setup for geophysical characterization of soil horizons in the calibration pit.

moisture increased from 15% to 45%, a regular and weaker soil resistivity decrease was remarked. However, these relationships obtained in laboratory were not representative because the saturation water conductivity of the soil cores was different from the natural soil solution electrical conductivity in the field. Moreover, we observed a high variability of the soil core electrical resistivity measurement with the soil sample volume. For the same moisture, an increase in the soil core volume was always associated with a higher electrical resistivity value, which suggests that the measurement elementary volume of the soil core must be defined before using a laboratory relationship. Because of this major limitation, we decided instead in this study to develop a field-scale site specific petrophysical model, which we judged to be more representative of natural conditions.

[17] The aims of this field study were (1) to verify that soil moisture changes generate measurable electrical resistivity changes, (2) to set up a simple field-scale calibration relationship for each soil horizon enabling the calculation of soil water content as a function of its temperature and electrical resistivity, and (3) to use these relationships with time-lapse ERT data to estimate moisture content variations over time at the field scale.

[18] This calibration was performed with a monitoring device implanted in a calibration pit (Figure 3) dug into the Calcisol very near of the experimental plot. The electrical resistivity of the soil horizons was measured by a Wenner electrode array with an electrode spacing of 0.15 m. The electrodes were driven horizontally into the wall of the pit over a length of 0.35 m at 0.18 m, 0.50 m, and 1 m depths as illustrated in Figure 3. Only the extremities of the electrodes were in electrical contact with the soil enabling a point measurement of electrical potential and point injection of electrical current in an infinite medium. The geometry of the quadripoles allowed most of the current lines to remain in each studied soil layer. The water content and temperature of the three soil horizons were measured with TDR probes and platinum-wire thermal probes respectively. After installation of the different sensors, the soil pit was carefully refilled, horizon by horizon. To limit the disruptive effects of the soil structure deterioration caused by the excavation, the monitoring began more than 6 months after the installation of the sensors and lasted one year. The various synchronized measurements were made on average every two weeks (Table 2). Thirty measurements were made on dates likely to show the various soil moisture states.

[19] The value of the electrical resistivity ρ of a medium that is assumed to be infinite and is measured with a Wenner electrode array with an inter-electrode distance a, is

$$\rho = 4\pi a(\Delta V/I) \tag{2}$$

where I is the intensity of the current injected between electrodes A and B and ΔV is the potential difference measured between electrodes M and N (Figure 3). The electrical resistivity was measured not only at different water contents but also at different soil temperatures. To eliminate the effect of the temperature and determine only the electrical resistivity and horizon moisture relationship, all the electrical resistivity measurements were corrected and related to a reference temperature of 25°C. The correction rule, adopted for a range of temperatures from 5°C to 25°C, corresponding to the maximal amplitude of the variation of the soil thermal profile, is a 2% per °C linear increase of the electrical conductivity of the soil with temperature [*Campbell et al.*, 1948; *Iliceto*, 1969] as the following relationship :

$$\frac{1}{\rho_T} = \sigma_T = \sigma_{25^\circ C}[1 + 0.02(\mathrm{T} - 25^\circ\mathrm{C})] \tag{3}$$

Table 2. Physical Parameters Measured During Both Monitoring Experiments

Experimentation	Experiment Site	Experiment Time	Physical Parameters Measured	Sensors or Experimental Setup	Interval of Measurement
Spatial and temporal monitoring of water flow	study area	10 days	electrical resistivity ρ	dipole-dipole electrical resistivity tomography	1 hour during a 36 hours period, then irregular
			water content θ	TDR probe	20 minutes
			temperature T	Platinum wire thermal probe	1 hour
			irrigation water amount	rainfall recorder and rain gauges	continuous measurements
Geophysical characterization of Calcisol horizons	calibration pit	1 year	electrical resistivity ρ	Wenner quadripole	15 days
			water content θ	TDR probe	15 days
			temperature T	platinum wire thermal probe	15 days

with ρ_T electrical resistivity at the temperature T (in Celsius degree), σ_T electrical conductivity at the temperature T, $\sigma_{25°C}$ electrical conductivity at 25°C.

[20] Linear regression was used to determine the specific relationships between water content and electrical resistivity of the three typical Calcisol horizons measured in the calibration pit (Figures 3 and 4). The literature and laboratory measurements showed that polynomial function (power 2) or power function were must commonly used for a large range of moisture changes ranging between full saturation and dry soil states. However, for low volumetric water content changes ranging from 20% to 35% between the permanent wilting point and the field capacity, which corresponds to natural soil moisture changes in the region, our laboratory measurements confirmed that the most simple linear relationship was overall sufficient for the all three soil horizons.

[21] The relationships between electrical resistivity and moisture of the three typical horizons of the Calcisol

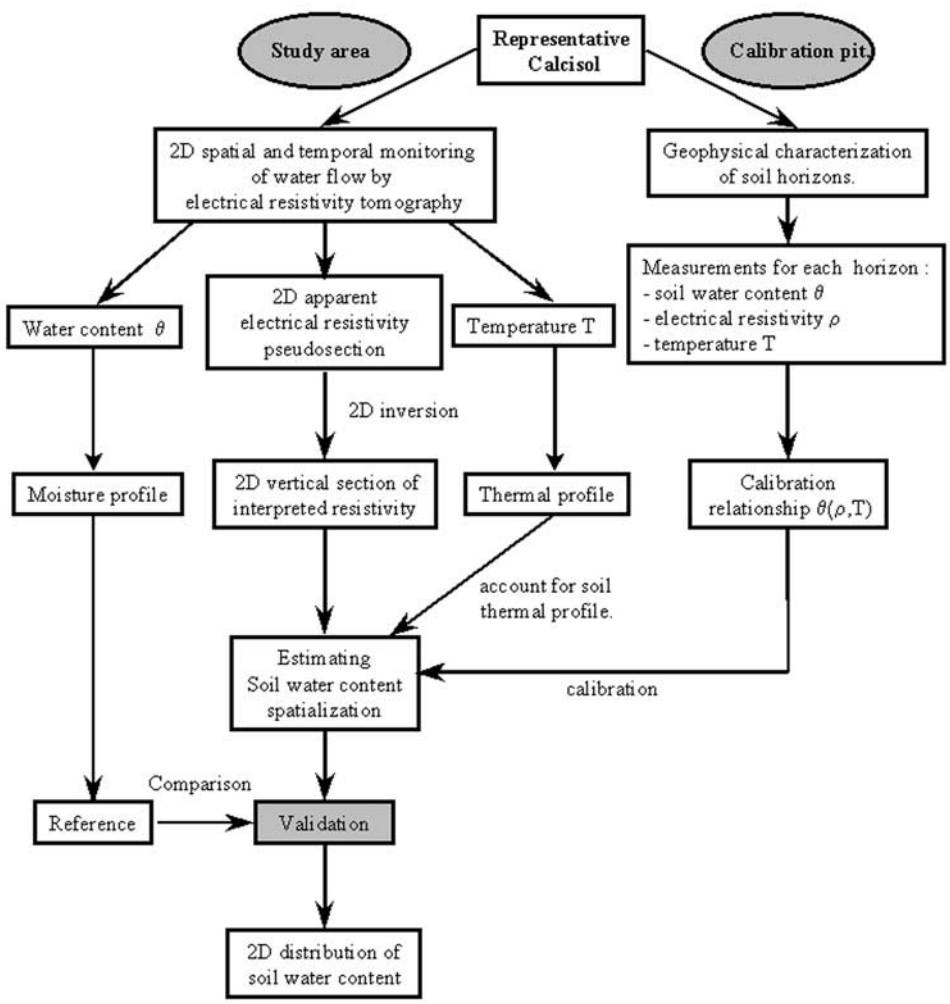

Figure 4. Diagram explaining procedures to monitor spatially and temporally the water flow by electrical resistivity tomography and to produce a 2-D soil water content tomography.

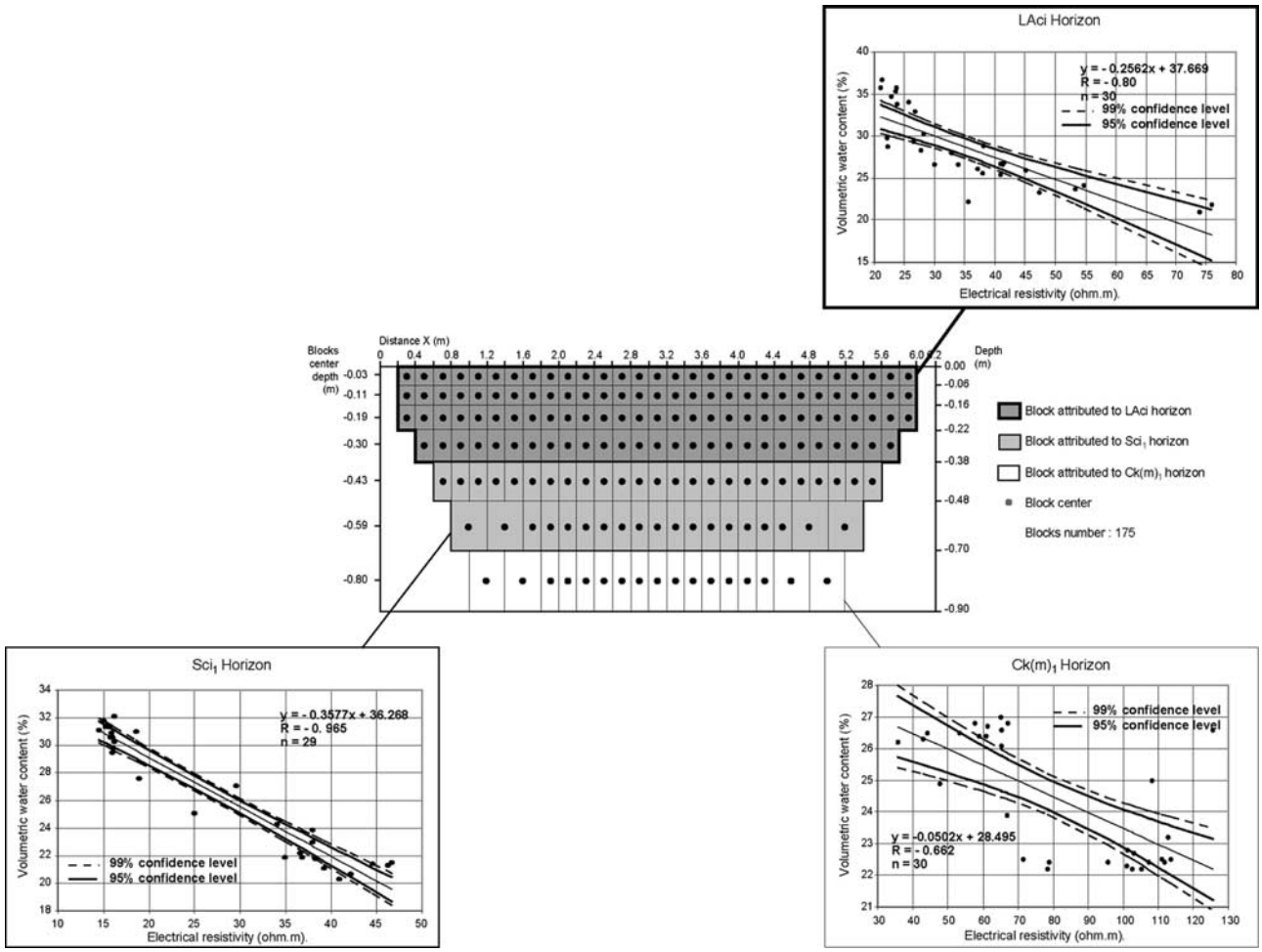

Figure 5. Calibration relationships (T = 25°C) between the moisture and the electrical resistivity of three characteristic soil horizons and schematic procedure of 2D soil water content section modeling using interpreted electrical resistivity model blocks.

showed and verified that in the explored domain, electrical resistivity increased linearly with decreasing water content. Nevertheless, the slope and the sensitivity of the relationship varied depending on the soil horizon under consideration (Figure 5). The linear relation between moisture and electrical resistivity of the horizons was quantified by their correlation coefficient **R** (Table 3). A quality index $|\Delta \mathbf{R}/\mathbf{R}|$ representing the ratio between the confidence interval of the correlation coefficient $\Delta \mathbf{R}$ for a 5% error margin and the correlation coefficient **R** enabled the relationships to be classified. When the $\Delta \mathbf{R}$ was high and $|\mathbf{R}|$ was low, a high index value showed an inferior quality of the relationship. Inversely, if $\Delta \mathbf{R}$ was restricted to a high value of **R** close to 1, a low value of the index indicated a high quality relationship.

[22] The loamy clay horizon Sci_1 displayed the best linear relationship. The coefficient **R**, for a confidence level of 95%, ranged between the values of −0.98 and −0.92. The quality index, with a value close to zero, was the lowest of the studied soil profiles, which indicated the highest quality calibration relationship. The sensitivity, corresponding to the inverse of the slope absolute value, was 2.8 Ωm by percent of soil volumetric water content. Nevertheless, the electrical resistivity measured was lower than those measured in the laboratory on cylindrical soil cores with the same moisture range [*Michot et al.*, 2001] and furthermore, the sensitivity of 2.8 Ωm was clearly higher than that observed in the laboratory which was 1.7 Ωm by percent of soil volumetric water content. This could be explained either by a difference between the volume measured in the field and that of the samples, by the disturbance due to the transport of the sample in laboratory, or by variability in the samples.

[23] The plowed surface horizon, LAci, displayed a linear relationship characterized by a coefficient **R** = −0.80, taken between −0.64 and −0.90 for an accepted confidence level of 95%. The sensitivity of the relationship was 3.9 Ωm by percent of soil water content. Considering the data, a power 2 polynomial function seemed appropriate too. However, a residual analysis showed that was not significant improve-

Table 3. Summary Statistics to Quantify the Linear Relationship Between Moisture and Electrical Resistivity of Three Calcisol Horizons

Soil Horizon	n	R	R_{min}	R_{max}	$\lvert\Delta R/R\rvert$
LAci	30	−0.80	−0.90	−0.64	0.32
Sci_1	29	−0.96	−0.98	−0.92	0.06
$Ck(m)_1$	30	−0.66	−0.80	−0.39	0.65

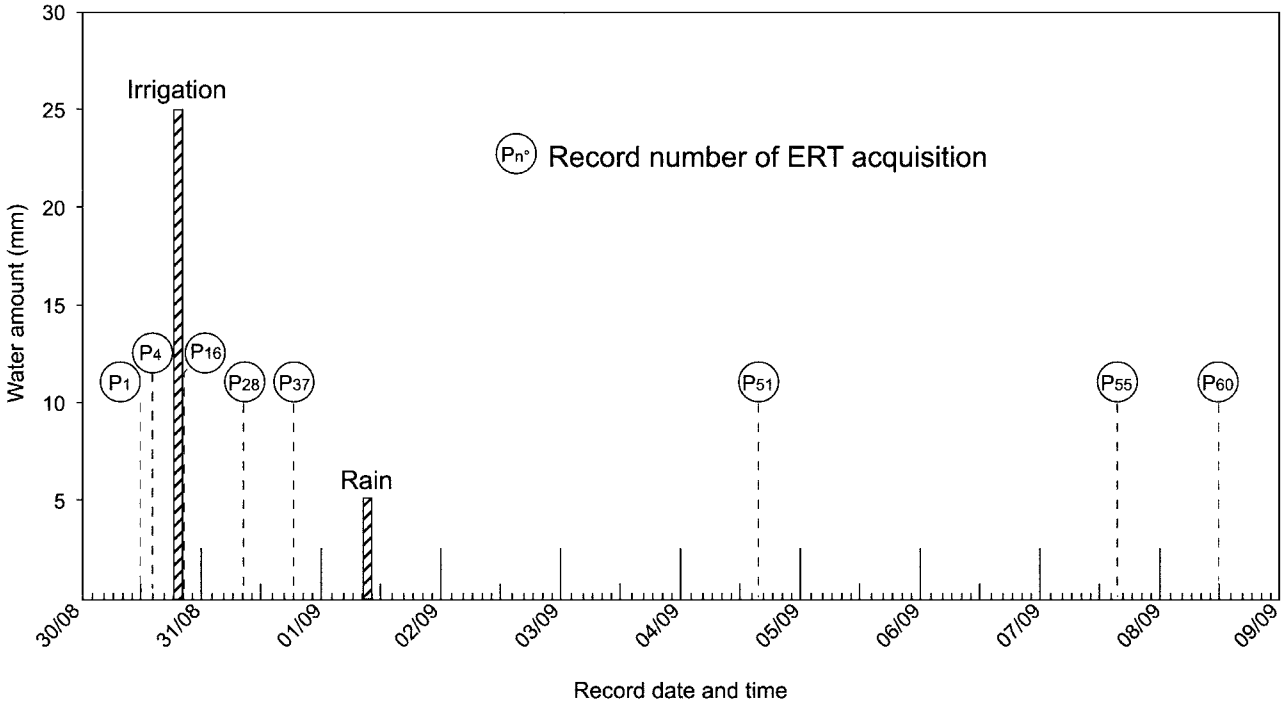

Figure 6. Electrical tomography, natural rainfall, and irrigation water depth records over time.

ment of this curve fitting in comparison with a linear relationship. Both small range of resistivity and moisture changes explained that a good fit of such a curve could not be obtained. On the field, we have not access to soil water content extreme values as in laboratory. So, we do not have any reason to choose a power 2 polynomial function. A linear relationship was sufficient.

[24] The linear relationship observed in the cryoturbated calcareous horizon of $Ck(m)_1$ presented the lowest correlation coefficient and the highest quality index of the three Calcisol horizons. For a small water content change, the apparent resistivity data were relatively dispersed. Because of this major limitation we used only a linear relationship. The heterogeneity of the cryoturbated limestone horizon and the lower moisture variation in this horizon situated at a 1 m depth could explain the lower quality of the relationship. For a decrease in soil moisture of 5%, the resistivity of the horizon increased by 90 Ωm, *i.e.* a sensitivity close to 19.9 Ωm by percent of soil volumetric water content.

5. Monitoring

[25] The aim of this field study was to first acquire the resistivity data for later transformation in water content and secondly, to acquire point water content measurements for validation of the estimated water content (Figure 4). For this second purpose a second pit was dug near the monitoring study area (Figure 2).

[26] This data acquisition was carried out during an irrigation cycle, on a corn crop characterized by a regular implantation of corn plants in rows justifying a 2-D study. Two-dimensional soil electrical resistivity tomography data were acquired over time using a multielectrode method at the surface of the study area. Two-dimensional soil moisture profiles were then estimated from the 2-D ERT profiles using the calibration relationships previously established from stationary measures in the pit, as described in section 4.

[27] Temporal monitoring of the electrical resistivity, water content and temperature of a vertical soil section was carried out over a period of 10 days (Figure 6 and Table 2), before, during and after irrigation of the experimental plot by means of a rotating ramp fitted with sprinklers. Irrigation supplied 25 mm of water by sprinkling on the experimental device between 18h and 20h. On 1 September 2000, 5 mm of additional water is supplied by one hour of rainfall. The electrical conductivity of the irrigation water measured in 5 samples taken from 4 rain gauges and in the rainfall recorder ranged between 17.5 10^{-3} S m^{-1} and 19 10^{-3} S m^{-1} (Table 4).

5.1. Electrical Resistivity Measurement and Interpretation

5.1.1. Electrical Device and Data Acquisition

[28] Resistivity measurements were carried out with the resistivity meter Syscal R1 (Iris Instruments, Orléans, France) equipped with 32 electrodes. The intensity and

Table 4. Electrical Conductivity of Irrigation Water Samples

		Rain Gauge			
	Rainfall Recorder	1	3	4	5
Sample volume (cm^3)	975	550	245	220	495
Electrical conductivity (S m^{-1})	18×10^{-3}	19×10^{-3}	19×10^{-3}	17.5×10^{-3}	17.5×10^{-3}

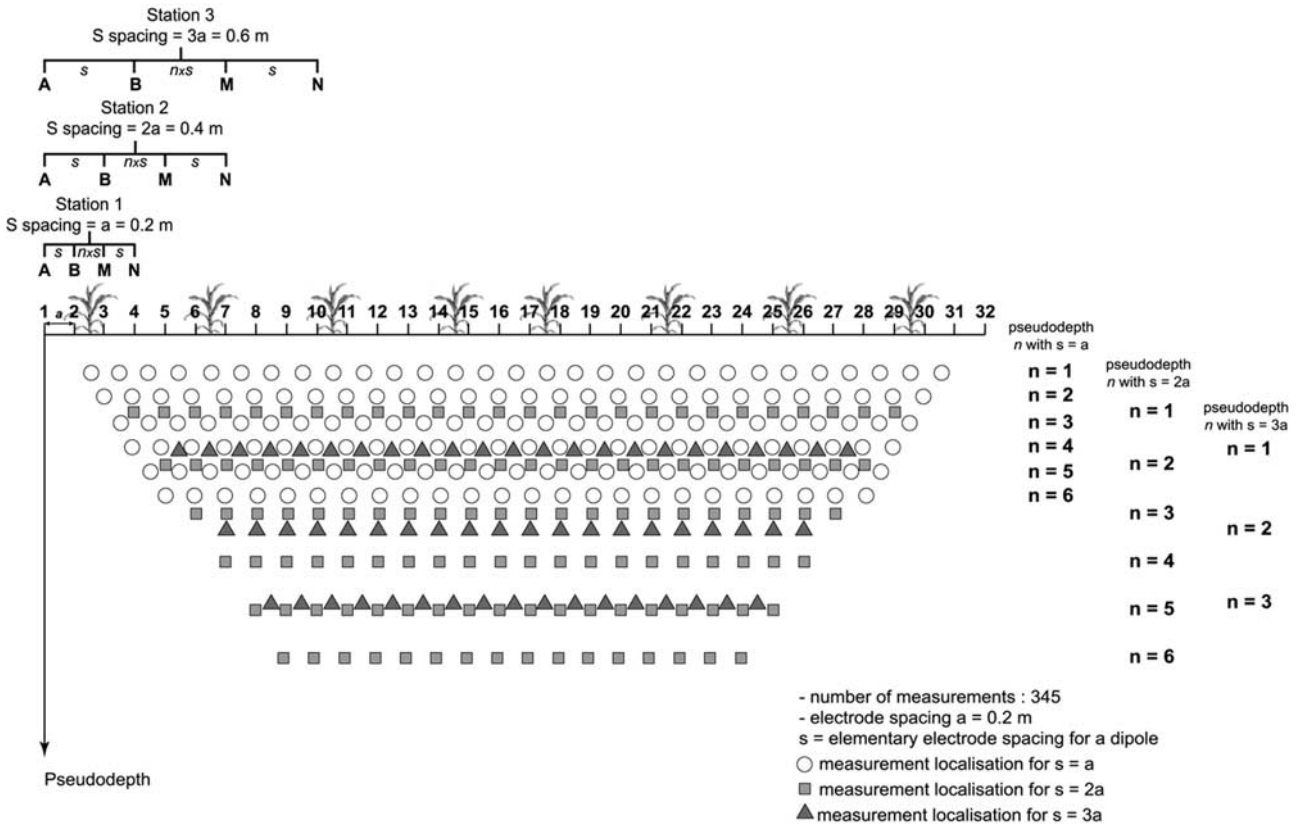

Figure 7. Measurement sequence to construct a pseudosection using a dipole-dipole multielectrode setup. Measurements are shown on a vertical plane.

voltage accuracy is 0.3%, which is consistent with the measurements carried out under constant surface conditions. Repeated measurements in stable hydrogeologic conditions for about ten hours were persistent within a tenth of an ohm-meter, i.e., one thousandth of the measured resistivity. During sprinkling, variations of the measured resistivity could reach several ohm-meters between two sets of measurements 1 hour apart. The electrodes remained on the soil surface during all the experiment time to avoid any electrode polarization changes and to ensure a best quality of measurements.

[29] The experimental setup included a row of 32 electrodes, lined up on the soil surface (Figure 2), in a direction perpendicularly to 8 corn rows, which were separated by 0.8 m. This device had a total length of 6.2 m with an electrode spacing (**a**) of 0.2 m. The dipole-dipole arrangement was chosen because it allowed the greatest number of measurements for a given number of electrodes, which was advantageous for data inversion. Moreover, the dipole-dipole array was very sensitive to horizontal changes in resistivity, but relatively insensitive to vertical changes in resistivity. That means that it was convenient in mapping vertical structures, such as water preferential flow direction induced by soil cracks. For each resistivity measurement, electrical current was injected between two adjacent electrodes (dipole A B) and the difference potential was measured between two others neighboring electrodes (dipole MN). A preprogrammed measurement sequence (Figure 7) was implemented in the resistivity meter and the multiplexer provided electrode commutation. To obtain the best resolution, especially down to 0.50 m depth, 345 measurements, located at 15 levels of investigation, were made during each sequence. The first 6 levels (**n**) were characterized by a spacing (**s** = **a**) between electrodes of each dipole. For each of these 6 levels (**n**), the spacing between dipoles was (**n** × **s** = **n** × **a**). One possible disadvantage of this array was the very small signal strength for large values of the (n) factor, the voltage being inversely proportional to the cube of the (n) factor. This means that for the same current, the voltage measured by the resistivity meter dropped by about 200 times, when (n) was increased from 1 to 6. One method to overcome this problem, was to increase the (a) spacing between both electrodes of each dipole to reduce the drop in the potential when the overall length of the array was increased to increase the depth of investigation. So, to insure the measurement quality at depth with a high signal/noise ratio, 6 new levels (**n**) were investigated with a spacing (**s** = **2a**) between electrodes of each dipole. For the same reason, the measurements at the last 3 levels were made with a spacing (**s** = **3a**). By convention, each apparent electrical resistivity measurements were located at the quadripole center and at a depth proportional to both dipole spacing.

[30] Each ERT sequence took just under one hour to acquire. During the first 36 hours of space-time monitoring of the water flow, the resistivity was monitored at regular intervals of 1 hour, then at increasing intervals (Table 2).

5.1.2. ERT Processing

[31] Inversion of the measured resistivities is an essential step before interpretation because the raw resistivity mea-

surements rarely give the true structure of the soil. *Panissod et al.* [2001] showed that the 2-D inversion was appropriate in this case according to a 3-D inversion. Indeed, a 3-D modeling using both finite difference and moment-method confirmed the reality of 2-D artifacts, showed that 3-D effects were not significant and allowed us to exclude numerical artifacts. So inverted resistivity sections were achieved with the RES2DINV software [*Loke and Barker*, 1996]. This technique was based on the smoothness-constrained least squares method and it produced 2-D subsurface model from the resistivity section. In the first iteration, a homogeneous earth model was used as starting model for which the resistivity partial derivative values could be calculated analytically. For subsequent iterations, a quasi-Newton method was used to estimate the partial derivatives which reduced the computer time. In this method, the Jacobian matrices for a homogeneous earth model was used for the first iteration, and the Jacobian matrices for subsequent iterations were estimated by an updating technique. The model consisted of a rectangular grid. The software determined the resistivity of each mesh which gave a calculated electrical resistivity section according to field measurements. The iterative optimization method attempted to reduce the differences between measured resistivity values and those calculated with the inversion model. The difference was estimated by the root mean square error (RMS error). Topographic correction was not taken into account for this inversion process, and each ERT was inverted independently. The model obtained from the inversion of the initial data set was not used as a reference model to constrain the inversion of the later time-lapse data sets, as it was possible with the recent version of RES2DINV software. A minimum of 5 successive iterations were made. However, for ERT inversions, the same number of data and mesh of the model were conserved, so the inversion of each ERT data was not totally independent.

[32] Each measured resistivity section was inverted. Water infiltration was indicated by variations in electrical resistivity of the soils, as expected [*Ward*, 1990], i.e. electrical resistivity in the soils decreases when the soil water content increases, and vice versa. To enhance the representation of that occurrence, sections of resistivity changes were calculated in relation to some sections measured at typical moments representative of particular hydric soil states. In this manner of calculating ''difference images'', water infiltration was studied in relation to the first ERT (P1, Figure 6) measured at the initial soil moisture state at the beginning of the experimental monitoring. Soil desiccation by evapotranspiration was observed by comparison to an ERT (P37, Figure 6) made after irrigation of a wet soil, near field capacity, whose moisture profile was therefore considered stabilized.

5.1.3. Procedure for Soil Moisture Estimation Using ERT Data

[33] The water content section was shaped from the rectangular grid network of the 2-D ERT data established during geophysical inversion. The vertical rectangular grid (Figure 5) was composed of 175 rectangular meshes localized by their central coordinates (X, Z). X represents the horizontal distance along the electrode line and Z is the vertical depth of rectangular mesh center. The grid was divided into 7 layers, which depths were 0.03 m, 0.11 m, 0.19 m, 0.30 m, 0.43 m, 0.59 m and 0.80 m respectively.

[34] The calibration relationships obtained for the three typical Calcisol horizons were respectively attributed to the corresponding rectangular meshes. The relationship obtained between resistivity and water content of the plowed LAci horizon was used for the first four layers of meshes. The observed relationship on the median structural horizon Sci_1 was used for the next two layers of meshes. Finally, the typical relationship of the mineral horizon $Ck(m)_1$ was used for the last layer of meshes. As the soil thermal profile was known at the moment of each electrical tomography measurement, the soil temperature at the center of each mesh was calculated by linear interpolation. For each one, the calibration relationship for the calculation of water content values was selected at the temperature nearest to the real soil temperature at this depth. The 2-D water content sections were then mapped by means of a triangulation method.

[35] To evaluate the quality of the soil moisture prediction, 349 water content values measured in the plowed LAci horizon by TDR probes were compared with those modeled from the electrical tomographies measured at the same time and with the same coordinates (X,Z) (Figure 4). The soil water contents modeled and compared with the TDR measurements were located either under the corn rows (X = 2.7 m and X =3.5 m), or between them (X = 3.1 m and X = 3.9 m). As only the rectangular meshes situated at depths of Z = 0.1 m, 0.19 m and 0.3 m corresponded to the TDR implanted at respectively 0.10 m, 0.20 m and 0.30 m depths (Figure 2), the modeled and observed moistures were only compared in the plowed LAci horizon. Thus 96, 126, 127 moistures content measurements and estimates were compared at the respective depths of 0.10 m, 0.20 m and 0.30 m.

5.2. Measurements of Soil Water Content and Soil Temperature Using Conventional Approaches

[36] Soil volumetric water content and soil temperature were estimated and measured, simultaneously during ERT acquisition using point measuring devices. Four moisture profiles were monitored over time using 18 TDR probes.

[37] Two moisture profiles were studied directly beneath a corn row (rows R4 and R5), and two others were located between two rows (row spacings R4–R5 and R5–R6). The TDR probes were set at 0.1 m, 0.2 m, 0.3 m, 0.5 m and 0.7 m depths in loamy clay horizons. Moisture profiles were measured at 20 min intervals. Thermal soil profile changes were monitored by 5 platinum-wire thermal probes (PT100). Soil temperature was measured at 0.1 m, 0.2 m, 0.5 m, 0.7 m and 1 m depths (Figure 2). Thermal profiles were measured every hour (Table 2). At the soil surface, a rainfall recorder registered the times and rates of sprinkler irrigation. Five rain gauges measured the amounts of irrigation water. Two rain gauges were situated underneath corn rows and three others between corn rows.

[38] The distribution on the soil surface of water droplets from rainfall or sprinkler irrigation depended both on the aerial parts of the corn plants and on the local topography. This topography was the result of farming practices, mainly tractor wheel ruts. Water accumulated on the soil surface during irrigation, formed puddles and water flows along the ruts on the slope as streamlets. The rate of water infiltration into the soil was therefore lower than the sprinkling rate. In

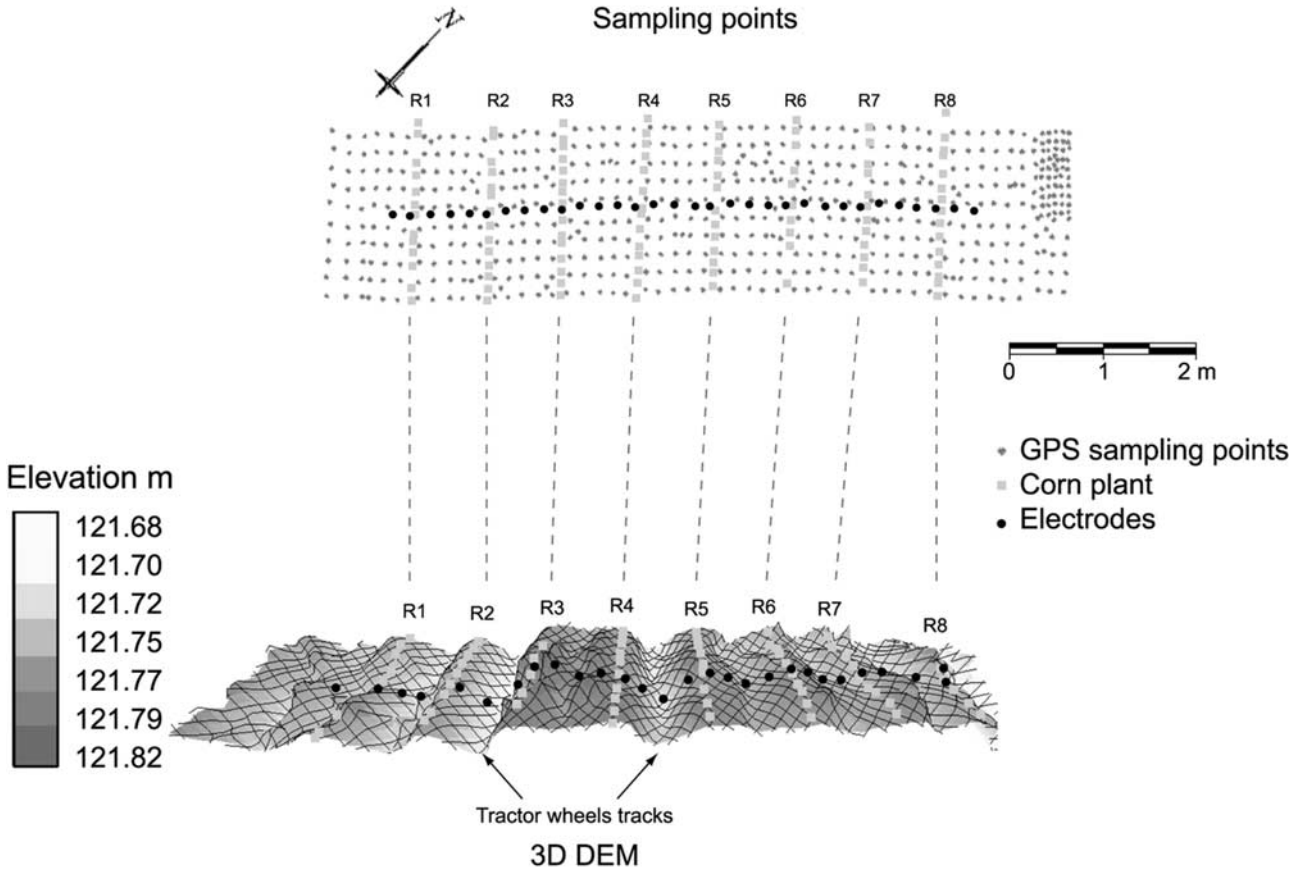

Figure 8. Elevation sampling points and digital elevation model (DEM) of the experimental plot.

order to study the role of topography in the location of preferential infiltration sites, a detailed topographical survey was carried out. The experimental plot selected in the corn field was an 8 m by 2 m rectangle. The slope was less than 2% and the corn row orientation followed the slope (NW/SE). A detailed digital elevation model (DEM) (Figure 8) of the experimental plot was built with the help of a high-performance global positioning system (GPS): Aquarius, from Thalès Navigation. The altitude survey was made in real time by a GPS working in a differential mode. The quality of the system allowed very fast measurements: in a few seconds a point was located with a precision of less than 1 cm. Measurements were taken atop a 2.50 m pole in contact with the ground surface to avoid any interference from the corn foliage. A grid marked on the ground insured a regular 20 cm spacing of the sampling points. During the topographical survey, 603 altitude measurements were recorded over a 16 m^2 surface. The positions of every corn plant and each electrode of the geophysical measuring device were precisely recorded. The DEM (Figure 8) was computed with Arc-Info software and its Grid module (ESRI). A network of points, with a 5 cm spacing, was built by a triangulation interpolation method.

6. Results

6.1. Evolution of the Thermal and Hydric Profiles

[39] The moisture profiles measured using TDR probes during the monitoring under the corn rows or between them showed varying infiltration as a function of depth and location (Figure 9). Under the corn rows, the volumetric moisture profiles showed the effect of irrigation with a moisture increase of more than 10% in the plowed horizon. After irrigation, superficial drainage occurred in the horizon with a progressive decrease in surface moisture and an increase by infiltration of the water content in the Sci_1 horizon at 0.5 m depth. The infiltration was clearly noticeable and instantaneous under corn row R4 with a moisture increase of nearly 5%. It was less significant under row R5 where the water content remained constant at a 0.5 m depth. Later, the moisture profiles under the corn rows progressively returned to their initial state. Finally, at the depth of 0.7 m, there was no change in soil moisture. When irrigation began, the usable water reserves were by no means exhausted in the LAci horizon but also in the median Sci_1 horizon where plant roots decreased (Table 5).

[40] The situation was different between the rows. Before irrigation, the moisture content was high, mainly between corn rows R4 and R5, nearly at field capacity. In the cultivated upper horizon, the moisture increased by about 5% as did the irrigation but this increase was lower than that observed under the corn rows. During the drainage and after irrigation, the moisture profiles measured between rows remained relatively constant over time. The water did not appear to infiltrate further down than the plowed horizon between rows R5–R6 and infiltrated only slightly between rows R4–R5 (Figure 9).

[41] The temperature variation did not seem to be directly related to variations in water content, apart from a decrease

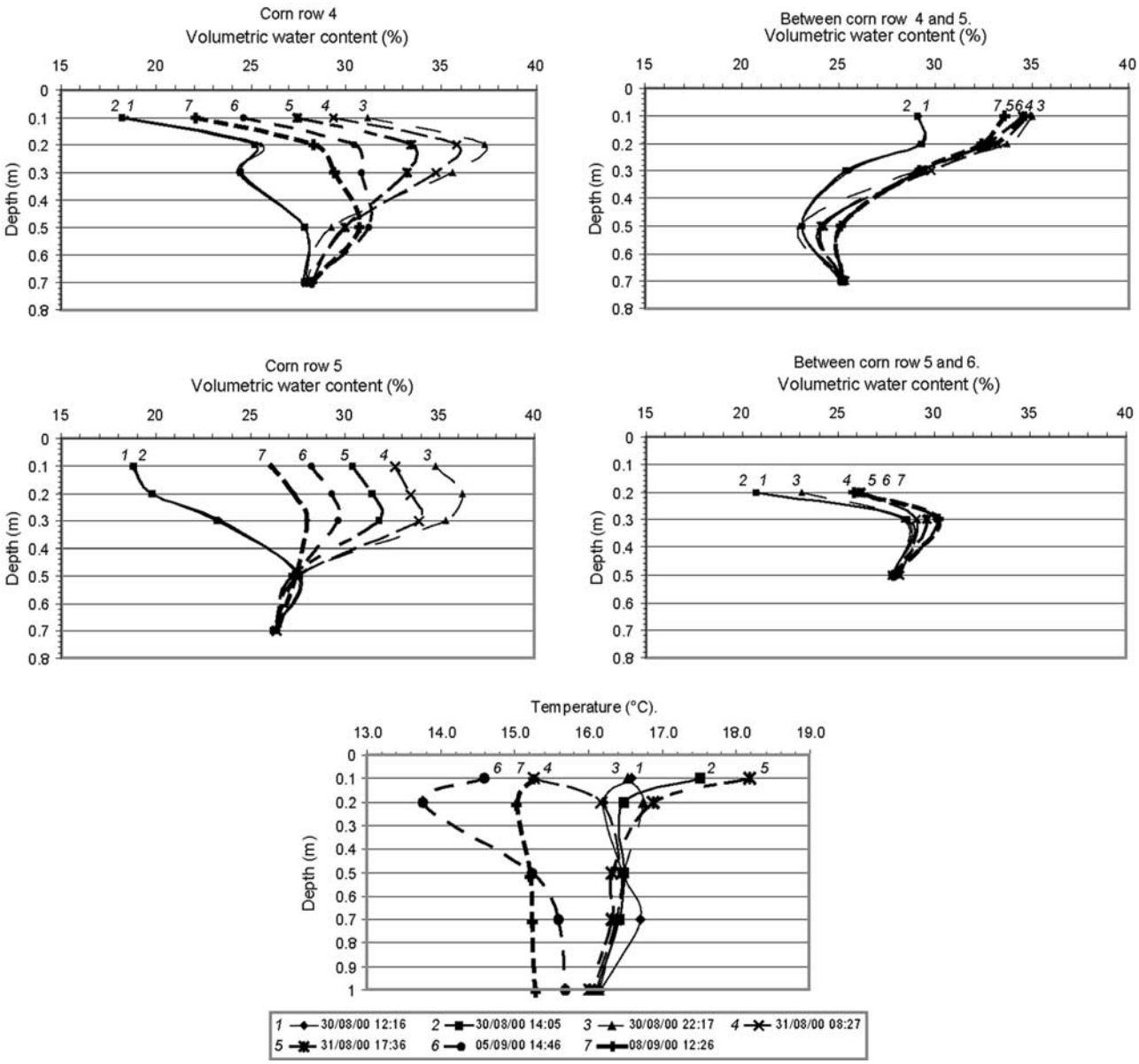

Figure 9. Volumetric moisture and thermal profile changes over time.

in temperature of 1°C at a 0.1 m depth just after the beginning of irrigation (curve 3). The thermal profiles were difficult to interpret. The daily cycle probably influenced the soil temperature at the time of the electrical data acquisition. Moreover, the platinum-wired thermal probes were not located in the same vertical plane (Figure 2).

6.2. Soil Hydric Fluxes Characterization From ERT

[42] Two-dimensional soil water content sections were then estimated using the ERT data, the calibration relationships between the electrical resistivity, the water content of the three horizons typical of the Calcisol (Figures 4 and 5), and the soil thermal profile. The last stage of processing consisted of testing the quality of the model soil moisture prediction by comparing measured and calculated water contents along the 2-D profiles.

[43] Sixty ERT profiles were acquired. In the context of this work, only eight ERT profiles (P1, P4, P16, P28, P37, P51, P55, and P60; Figure 6), which were particularly representative of moisture stages, were presented (Figure

Table 5. Calcisol Horizons Volumetric Water Content Measured at Different Soil Water Potentials (pF)[a]

Horizon	Depth, m	pF = 1	pF = 2	pF = 2.5	pF = 3	pF = 3.5	pF = 4	pF = 4.2	Field Capacity
LAci	0.10–0.20	42.4	39.6	35.7	31.2	27.4	21.3	20.2	36
Sci_1	0.35–0.45	38.1	34.4	31.7	26.7	24.2	20.9	20.1	35.2
$Ck(m)_1$	0.88–0.98	33.8	33.2	29.04	24.2	18.5	12.3	10.9	31.2

[a]The term pF can be obtained from the soil matric potential ΨM according to the formula pF = log(−ΨM). Water content is in percent.

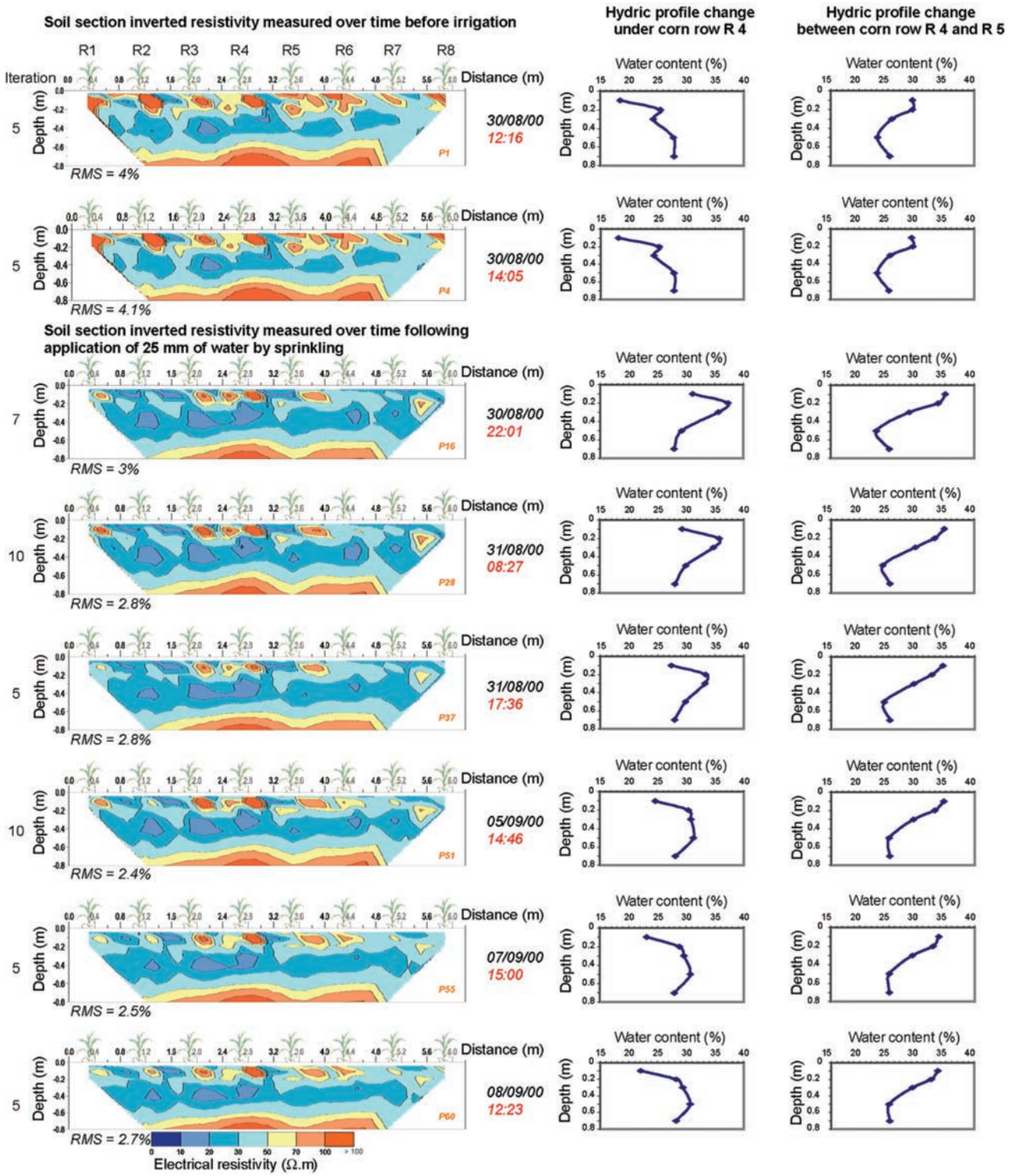

Figure 10. Characteristic true soil sections resistivity and volumetric moisture profiles measured over time during water infiltration after sprinkling and subsequent soil drying phase.

10). For each ERT section, two moisture profiles were indicated. The first moisture profile was obtained just under the corn row 4, while the second one was measured between rows 4 and 5. The section P1, measured at the beginning of the experiment, just before irrigation at 12:16 P.M. on August 30th, characterized the initial soil moisture state defined as reference.

6.2.1. Initial Soil Moisture State

[44] In the section P1 (first row of Figure 10), the main typical soil horizons were identified by their electrical resistivity. The first layer between the soil surface and the 0.3 m depth corresponded to the plowed LAci loamy-clay layer. It appeared to have a moderate resistivity (20 Ω m < ρ < 70 Ω m), with resistive structures (ρ > 100 Ω m) under

each corn plant. According to the profiles of corn roots density (Figure 2) [*Nicoullaud et al.*, 1995], the major resistivity anomalies in the plowed layer indicated that the soil volume had dried as a result of corn root water uptake [*Michot et al.*, 2001]. The drying process in the plowed layer was not uniform. This effect was less intense between rows due to compaction by tractor wheels (X-coordinates 1.5 and 3.1 m). Soil compaction between the corn rows by agricultural machines was also visible on the DEM (Figure 8). Wheel tracks had modeled the soil microtopography. The fact that the zones between the corn rows were lower was evidence of their compaction, which was also shown by a higher apparent density of the plowed horizon between the surface and a depth of 0.1 m (Table 6). These compacted zones had a smaller root density [*Tardieu and Manichon*, 1987]. The systematically oblique variations in the electrical resistivity of the soil and the oblique orientation of the pockets of resistant soil within the plowed horizon seemed linked to the orientation of the plowing clods. However, the obliqueness of these structures could also be an artifact linked to the nonsymmetrical positioning of the electrodes in relation to the corn plants or to the meshing of the electrical resistivity section during inversion.

[45] The median soil layer corresponding to the Sci_1 horizon had the lowest resistivity. The high clay content (32%) of the horizon explained its high conductivity (Table 1). The gradual increase of electrical resistivity with depth was related to clay content decrease and to smaller water uptake by corn roots.

[46] At a depth of 0.7 to 0.75 m, a resistive layer appeared, corresponding to the $Ck(m)_1$ horizon composed of beige cryoturbated limestone.

6.2.2. Water Infiltration Phase

[47] After irrigation, monitoring of the water flows was performed using the relative variations of ERT sections (Figure 11). Before irrigation, the electrical tomographies P1 and P4 measured at a two-hour interval in the same moisture conditions produced closely comparable resistivities. In the absence of change in the moisture state of the soil, in particular at the greatest depths, the electrical resistivity measurements were reproduced.

[48] During the moistening phase after the application of 25 mm of sprinkled water, the progressive saturation of the plowed LAci horizon by infiltration explained the general decrease in soil resistivity.

[49] Selective infiltration occurred under the corn plants and not in the low zones, between the corn rows, where surface water had a tendency to accumulate due to the effect of the soil microtopography (Figures 8 and 11). The vertical anomalies of negative electrical resistivity changes observed under the corn rows corresponded to the preferential directions of water flow. The aerial parts of the corn plants played an important role in the catching of water droplets. The water ran down the length of the stem, causing first an increase in soil moisture, and then infiltration under the corn plants. The role of topography would therefore appear to be less important in water infiltration as the water hardly infiltrated in the low zones between the rows.

[50] Three resistive pockets in the LAci horizon between corn rows R3 and R4 persisted over time. This was explained by the local soil microtopography. The irrigation water did not infiltrate here but ran rapidly in the direction of the slope toward the low zones in the soil surface created by tractor-wheel tracks (Figure 8).

Table 6. Bulk Density (da) of Ploughed LAci Horizon Measured on Cylindrical Soil Cores Sampled Between the Soil Surface and 0.1 m Depth[a]

Location	da 1	da 2	da 3	Mean	Standard Deviation
Corn row R4	1.28	1.23	1.26	1.26	0.03
Between corn rows R4-R5	1.52	1.58	1.37	1.49	0.11
Corn row R5	1.27	1.19	1.26	1.24	0.04
Between corn rows R5–R6	1.56	1.30	1.34	1.40	0.14

[a]Soil core volume is 500 cm^3.

[51] Locally, the upper parts of the median Sci_1 horizon showed resistivities of less than 20 Ω m, with a 20 to 70% resistivity decrease compared to the initial soil conditions. The percolating water could reach the upper part of the horizon and accumulated in the pores of the horizon.

[52] Two vertical structures located between two corn rows were characterized by an electrical resistivity that was constant or slightly increased over time. These domains were separated by a distance of 1.6 m to 1.8 m, corresponding to wheel span of an agricultural machine. The base of the LAci horizon was probably compacted by the passage of an agricultural machine before the corn was sown as the wheel tracks corresponding to the compacted zones did not appear in the soil topography. Soil compaction was shown between corn rows R5 and R6 by a higher bulk density of the LAci horizon, which could reach a value of 1.56 (Table 6). Compaction of the plowed horizon by the wheels of agricultural machines significantly reduced the infiltration capacity of the soil. *Ankeny et al.* [1990] showed that the hydraulic conductivity of the soil was greatly reduced by the passage of the wheels and they attributed this to the destruction of the macropores by compaction. The compacting of the horizon could create a shadow zone preventing the vertical infiltration of the water. Similarly, water was collected between the rows and was evacuated down the slope as runoff. There were two possible explanations of soil electrical resistivity increase either a soil temperature decrease or a soil moisture decrease. However, a numerical simulation showed that a realistic soil temperature decrease of 1°C provoked by cold water infiltration nearby could not explain an electrical resistivity increase higher than 5%. At the same depth, the soil moisture changes under a corn plant could be very different and even inverse from those observed under the both compacted area because the water infiltrated to this depth with different velocities. Moreover, the soil moisture history could involve different hydric behaviors. The experiment performed a sudden soil moistening after a slow drying phase between two water sprinklings. Under the compacted horizon characterized by a low hydraulic conductivity the local wetting kinetic was asynchronous in comparison with the rest of the soil profile. Both these domains were always in a slow drying phase. So, the electrical resistivity increase could be explained by a local water content decrease.

6.2.3. Soil Desiccation Phase

[53] During the drying phase, after the drainage period, the soil pockets characterized by a high electrical resistivity

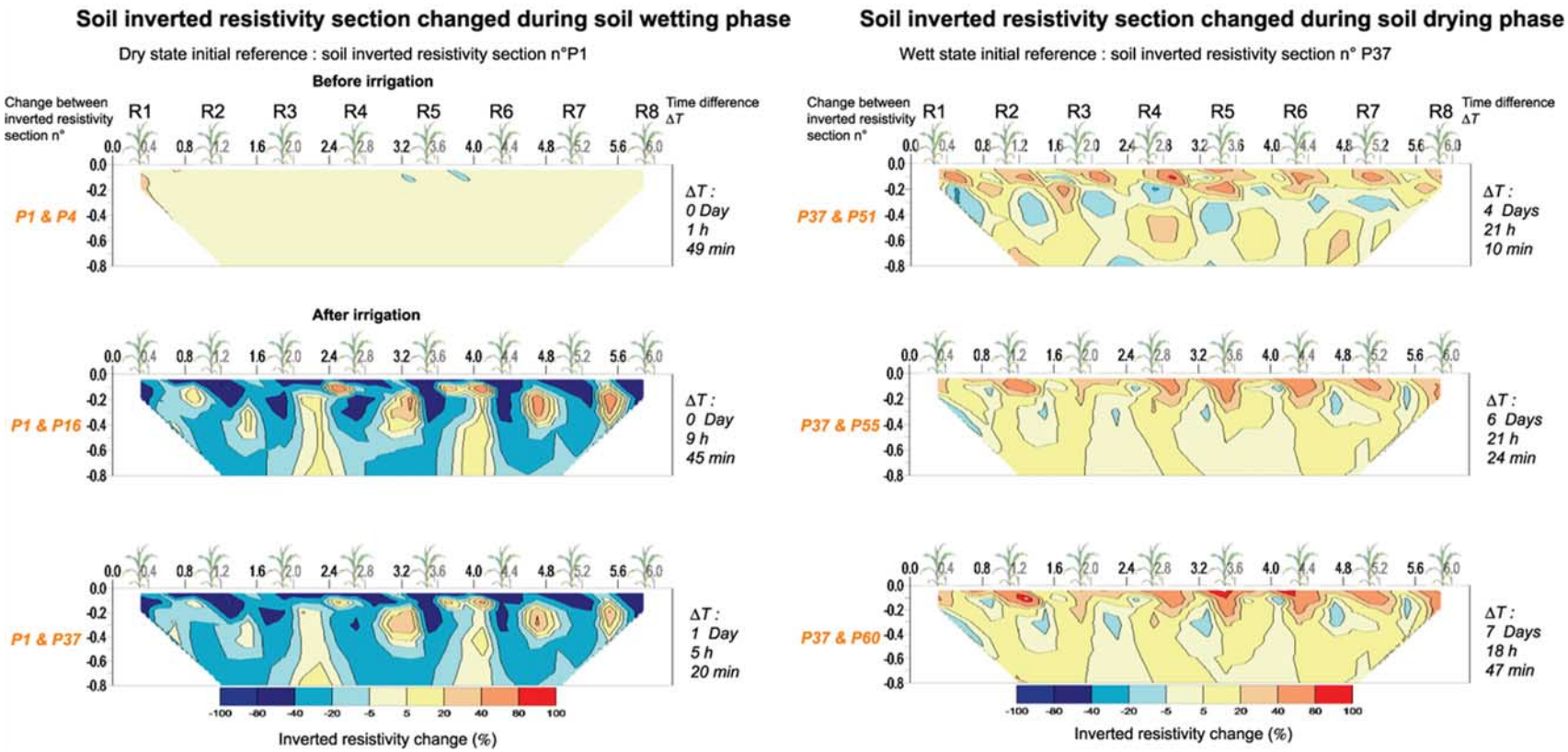

Figure 11. Soil sections of relative resistivity changes measured over time respectively during the soil wetting phase and subsequent drying phase.

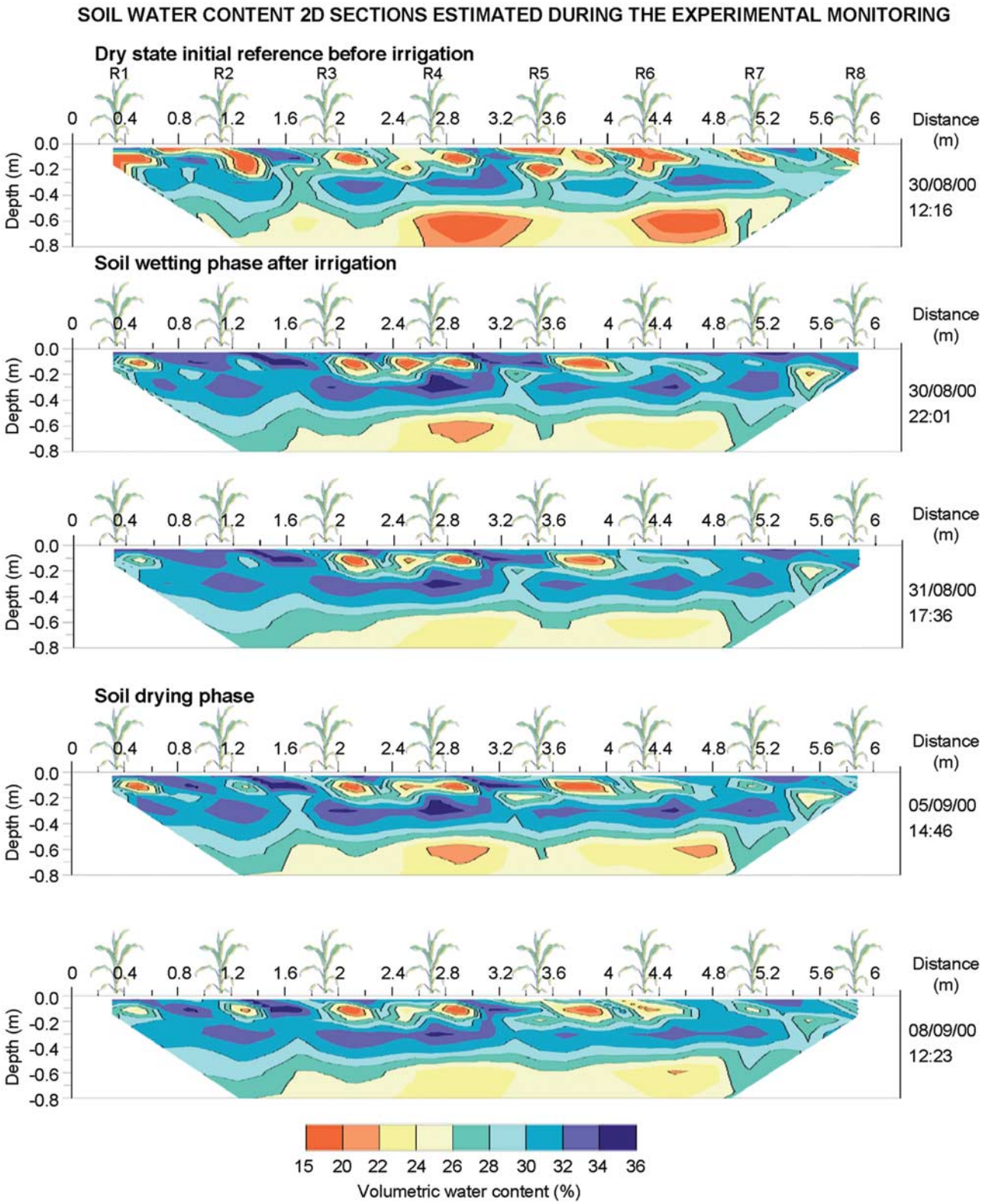

Figure 12. Characteristic soil moisture content sections computed over time during the experimental monitoring period.

reappeared under the corn plants in the LAci horizon (Figure 11). The size of the structures associated with the positive variations in electrical resistivity in relation to the electrical tomography P37 increased with time. The increase in electrical resistivity was first seen in the LAci horizon, then spread progressively downward. Soil pockets, drained by the corn root water uptake, were detected by an increase in the electrical resistivity of the soil. At the end of the monitoring period, the shape of the positive resistivity anomalies under the corn plants and the amplitude of the

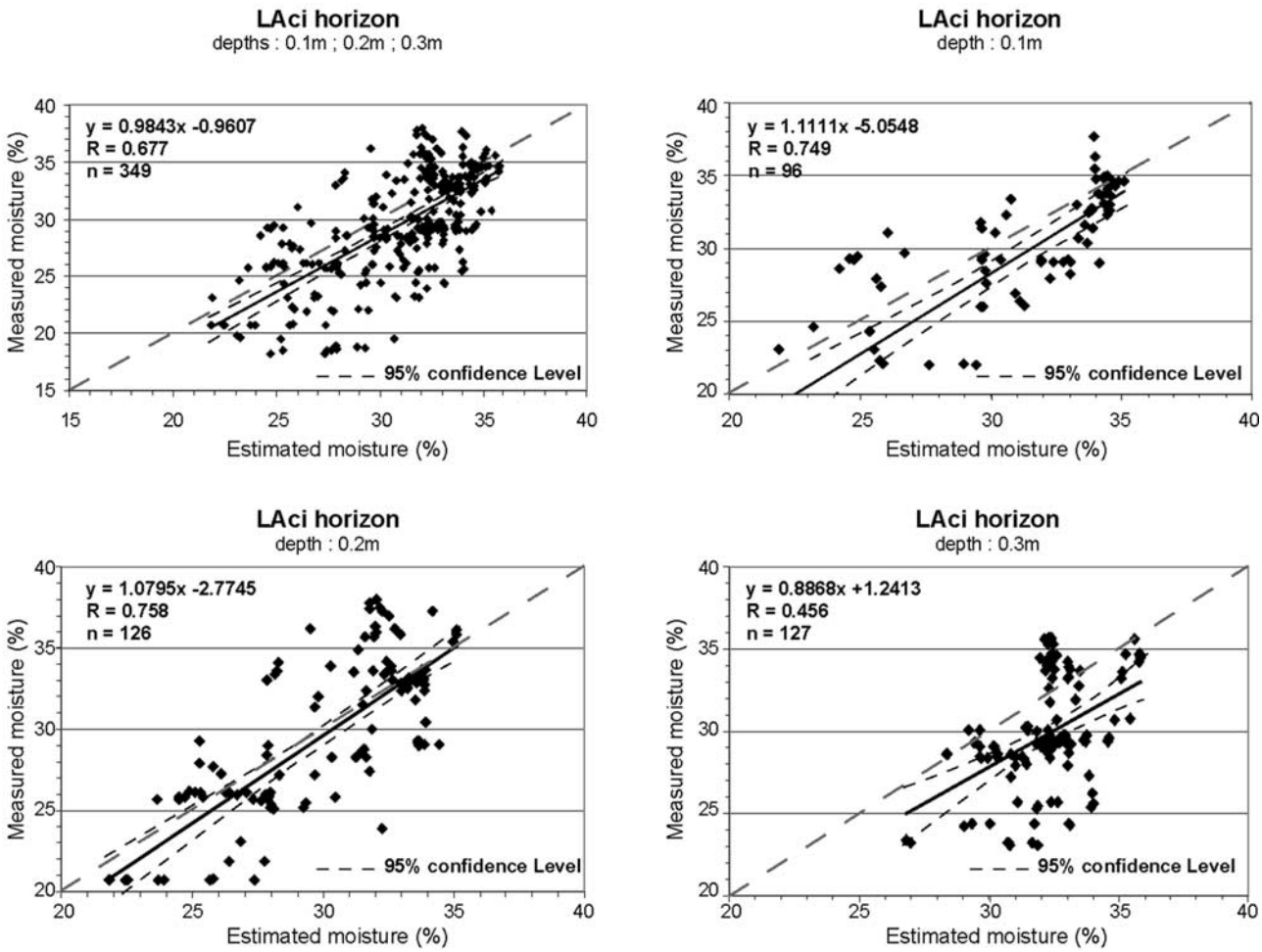

Figure 13. Validation: relationship between the moisture content of the ploughed horizon established by 2-D tomography and soil water content measured with TDR probes at the same time and the same location.

increase in electrical resistivity, evolved in the same way as the corn root frequency profiles : higher in the plowed horizon and lower at depth [*Nicoullaud et al.*, 1995]. To strengthen these observations and to retrieve information about root water uptake and soil water reserve from the time variations of resistivity, *Tabbagh et al.* [2002] have developed a model that solves simultaneously Richard's and heat conduction equations, and delivers for each time intervals the soil water distribution after sprinkling and the corresponding resistivity variations.

6.3. Soil Moisture Sections and Validation

[54] Five 2-D sections of moisture content of the selected soil, estimated using the ERT data obtained at various dates of the monitoring, are presented in Figure 12. The use of a linear relationship between moisture and electrical resistivity for the three soil horizons suggests that the spatial structure of the moisture sections and of the electrical resistivity sections are similar. The moisture sections reproduce the water flow previously revealed by variations in electrical resistivity during the phases of water infiltration and soil drainage.

[55] For the whole of the plowed LAci horizon, the water contents estimated using ERT data are effectively correlated with the measured values (R = 0.68) using TDR data (Figure 13 and Table 7). The slope of the linear regression between the modeled and measured water contents is close to the ideal value of 1. The estimate precision was quantified by the root mean square error (RMSE), while the estimation bias was quantified by the mean error (ME). The estimation bias is small and corresponds to an overestimation of 1.45% of the volumetric moisture. The precision of the water content estimation is 3.63%. The residual histogram, corresponding to the difference between the measured and calculated moistures, shows a Gaussian distribution of the residues (Figure 14). The histogram also shows that 26.5% of the residues range between −1% and +1% of volumetric

Table 7. Summary Statistics to Compare Soil Volumetric Water Content Estimated From Electrical Resistivity Tomography and That Measured With TDR Probes

Depth, m	n	R	ME, %	RMSE, %
0.1 to 0.3	349	0.68	−1.45	3.63
0.1	96	0.75	−1.59	3.85
0.2	126	0.76	−0.38	3.26
0.3	127	0.45	−2.40	3.80

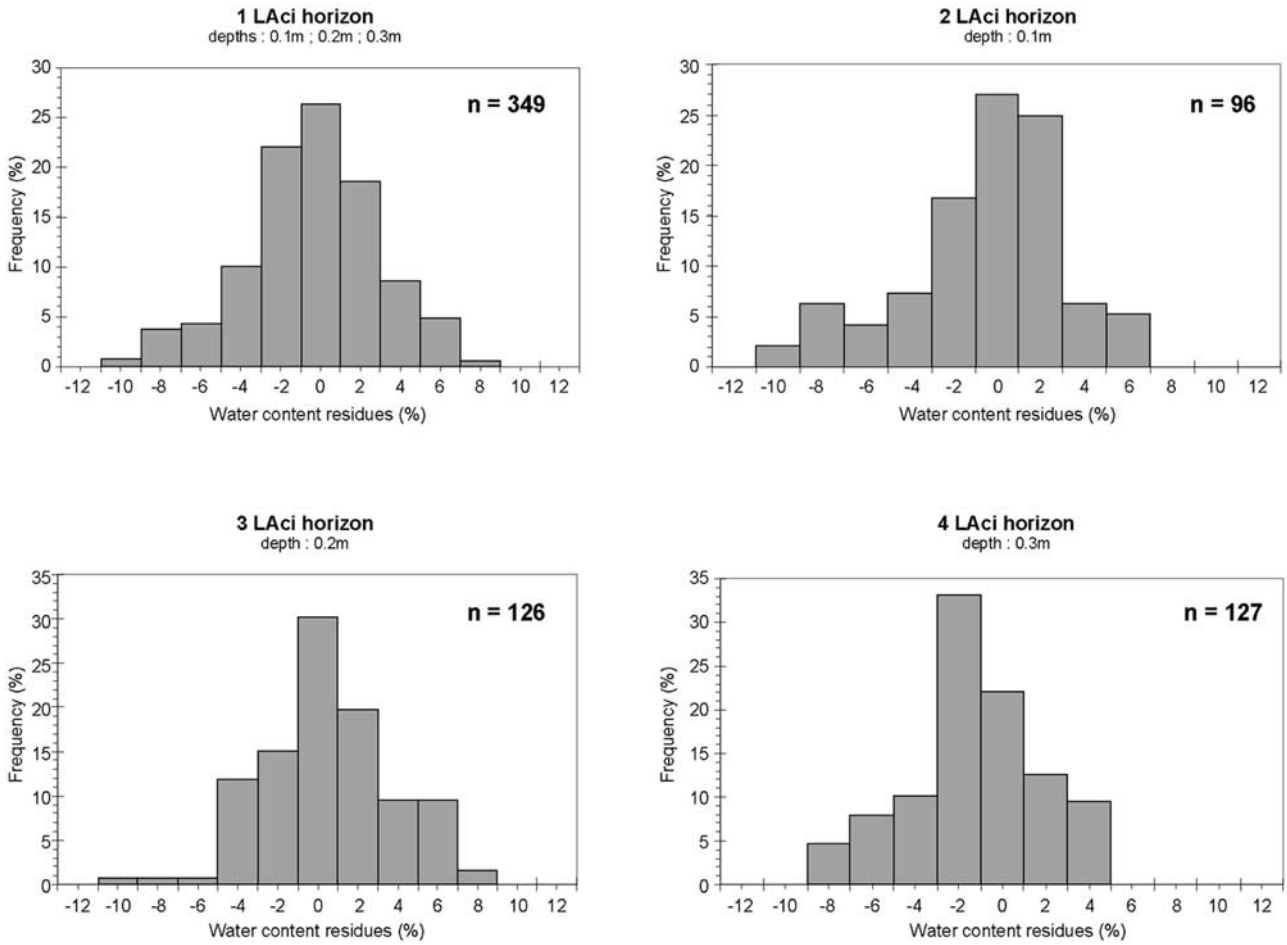

Figure 14. Residue frequency histograms between the ploughed horizon water content measured by TDR probes and soil water content estimated from electrical resistivity tomography measured at the same time and the same location.

moisture and that 67% of the residues are between −3% and +3% of volumetric moisture. The quality of the estimate of soil moisture is therefore satisfying.

[56] In Table 7, the highest correlation coefficient, the smallest bias and the greatest precision, reveal the best moisture estimation at a depth of 0.2 m.

[57] Conversely, at a depth of 0.3 m the correlation coefficient between the calculated and measured moistures is the lowest, the estimation bias the highest and the estimation precision the worst. At this depth, the moisture seems slightly overestimated as the majority of the estimation residues (33%) is between −3% and −1% of volumetric water content. The presence of the plowed pan at a depth of 0.3 m may explain this low correlation. The plowed pan constitutes the limit between the plowed surface horizon and the structural horizon Sci_1. At this level, the structure of the LAci horizon compacted by tillage is modified. The plowed pan is characterized by a major decrease in porosity and a modification of the hydrodynamic behavior of the horizon with a reduced infiltration. These changes explain why the calibration relationship of the LAci horizon is less adapted at this level and therefore why the correlation is lower.

[58] Several factors may explain the deviation between the soil water content estimation using ERT and measured by the TDR probes. (1) One is the distance of about 1 m separating the multielectrode device from the TDR profiles while soil moisture varies on a decimeter scale. (2) Another is the effect of the sides of the trench on the water flow. (3) The difference between the soil resistivity during the monitoring and the resistivity calculated by the 2-D ERT inversion procedure is another factor. The precision of the inversion and therefore of the estimation of the soil resistivity depends, among other sources of uncertainties, on the configuration of the electrodes, the interval between the electrodes and the number of measurements of the apparent resistivity of the soil. (4) Although small electrodes were used to reduce the contact resistance between the soil and the electrode, it is difficult to consider them as points which would be necessary for surveys requiring high resolution and shallow investigation depths. (5) The resistivity of soils may be subject to hysteretic phenomena. (6) As the conduction of current in soils is mainly electrolytic, soil resistivity depends not only on moisture and temperature but also on the ionic concentration of the studied soil solutions. During the experiment, the soil solution may be diluted by irrigation water pumped into a stratified aquifer with a significant TDS loading [*Schnebelen et al.*, 1999] leading to nonnegligible variations in the electrical resistivities. (7) The time (1 hour) needed to acquire a resistivity section is relatively long compared with

the infiltration rate of water during irrigation. A device permitting more rapid data collection must be considered in the future.

7. Conclusions

[59] Acquiring ERT data along a vertical soil section with a multielectrode surface method, which is nondestructive and spatially integrating, the boundaries of some soil horizons were delineated. Soil moisture changes over time were revealed by electrical resistivity changes in the soil. Two-dimensional soil water content sections were calculated from the ERT using field-scale calibration relationships between the electrical resistivity of each soil horizon and its water content. As the temperature variations in the soil affect the electrical resistivity of the water and therefore that of the soil, the thermal profile of the soil during the electrical resistivity measurements were taken into account in the calculation. A comparison of the modeled water contents with those measured by TDR probes confirmed that the reliability of a site-specific linear relationship between the calculated and measured moistures in the plowed LAci surface horizon. Overall, in the plowed surface horizon, the moisture estimates showed a precision of 3.6% for an estimation bias corresponding to a water content overestimation of 1.4%. The best estimation was obtained at 20 cm depth where the effects of both large surface moisture fluctuations and compaction of the plowed pan were attenuated.

[60] The hydraulic functioning of the soil was then monitored during a moistening/drying cycle. The drying out of the soil by corn root water uptake, the progression of the infiltration front after irrigation, the delimitation of preferential-flow zones and the surface drainage of the soil were identified and localized. At this stage of corn development (3 months), the parts of the soil involved in soil infiltration and drainage were mainly located directly under the corn rows. The corn plants played a major role in the redistribution of surface water before it infiltrated, while the role of the topography in water infiltration appeared to be limited. The particular structural characteristics of the soil horizons resulting from agricultural practices, and the notable effect of soil compaction due to the passage of agricultural machines were observed. In zones where the soil was compacted, moisture variations were negligible, which demonstrated the negative effects of compaction on water flow as well as on the possibilities of water storage.

[61] Measurements of soil water content using conventional tools typically sampling over small volumes, at wide intervals, and in an intrusive manner, are generally less representative than the actual and very complex situation of the soil moisture state. They do not allow a good monitoring of the evolution of soil moisture. Estimation of water content using ERT as a first approximation of the spatial distribution of soil water content in a cultivated soil is shown to be significant. Nevertheless, the validity of the proposed model could be limited to specific regional conditions such as loamy clay soils of the Beauce region.

[62] In the future, this method may allow verification of sprinkling irrigation efficiency and better estimation of the useful available water in the soil. Water spatial distribution is influenced by crop root distribution with depth, which is dependent on soil type and soil management as tillage operations. This method is a high-resolution investigation tool to study soil moisture and to perform soil water flow temporal monitoring.

[63] The development and adoption of precision farming and rational irrigation require a detailed knowledge of soils and crops [*Robert*, 1999]. This method is useful in research to describe the soil spatial variability and its hydric behavior with a high resolution. However, the precision is higher than the investigation level required in precision farming, and the requirement of an additional field calibration may render the method impractical for routine field use. The use of a general petrophysical relationship between the soil electrical resistivity and its moisture, if appropriate, could reduce the effort needed to make this a practical field tool for the purpose of improving irrigation management.

[64] **Acknowledgment.** We are grateful to the Associate Editor and to the anonymous reviewers for their constructive comments.

References

Aaltonen, J., Seasonal changes of DC resistivity measurements, paper presented at 3rd EEGS-ES Conference, Environ. and Eng. Geophys. Soc., Aarhus, Denmark, 1997.

Amin, M. H. G., R. J. Chorley, K. S. Richards, B. W. Bache, L. D. Hall, and T. A. Carpenter, Spatial and temporal mapping of water in soil by magnetic resonance imaging, *Hydrol. Processes*, *7*, 279–286, 1993.

Ankeny, M. D., M. Ahmed, T. C. Kaspar, and R. Horton, Characterization of tillage and traffic effects on unconfined infiltration measurements, *Soil Sci. Soc. Am. J.*, *54*, 837–840, 1990.

Archie, G. E., The electrical resistivity log as an aid in determining some reservoir characteristics, *Trans. Am. Inst. Min. Metall. Pet. Eng.*, *146*, 54–67, 1942.

Baize, D., and M. C. Girard, Solums carbonatés et saturés, in *Référentiel Pédologique*, pp. 109–120, INRA Ed., Paris, 1995.

Barker, R., and J. Moore, The application of time lapse electrical tomography in ground water studies, *Leading Edge*, *17*, 1454–1458, 1998.

Barraud, J. P., A. Dieulin, E. Ledoux, and G. de Marsily, Relation entre mesures géophysiques et flux de l'eau dans les sols non saturés, *Rapp. LHM/RD/79/3*, Ecole Natl. Supérieure des Mines de Paris, Paris, 1979.

Bavel, C. H. M., N. Underwood, and R. W. Swanson, Soil moisture measurement by neutron moderation, *Soil Sci.*, *82*, 29–41, 1956.

Beauce, A., J. Bernard, A. Legchenko, and P. Valla, Une nouvelle méthode géophysique pour les études hydrogéologiques: L'application de la résonance magnétique nucléaire, *Hydrogeologie*, *1*, 71–77, 1996.

Bell, J. P., T. J. Dean, and M. G. Hodnett, Soil moisture measurement by an improved capacitance technique, part II. Field techniques, evaluation and calibration, *J. Hydrol.*, *93*, 79–90, 1987.

Benderitter, Y., and J. J. Schott, Short time variation of the resistivity in an unsaturated soil: The relationship with rainfall, *Eur. J. Environ. Eng. Geophys.*, *4*, 37–49, 1999.

Binley, A., P. Winship, R. Middleton, M. Pokar, and J. West, Observations of seasonal dynamics in the vadose zone using borehole radar and resistivity, paper presented at the Annual Symposium on the Application of Geophysics to Engineering and Environnemental Problems (SAGEEP), Environ. and Eng. Geophys. Soc., Denver, Colo., 2001.

Bussian, A. E., Electrical conductance in a porous medium, *Geophysics*, *48*, 1258–1268, 1983.

Campbell, R. B., C. A. Bower, and L. A. Richards, Change of electrical conductivity with temperature and the relation of osmotic pressure to electrical conductivity and ion concentration for soil extracts, *Soil Sci. Soc. Am. Proc.*, *13*, 66–69, 1948.

Chanasyk, D. S., and M. A. Naeth, Field measurement of soil moisture using neutron probes, *Can. J. Soil Sci*, *76*, 317–323, 1996.

Clavier, C., G. Coates, and J. Dumanoir, The theorical and experimental bases for the "Dual water" model for the interpretation of shaly sands, paper presented at 52nd Annual Fall Technical Conference and Exhibition of the SPE of AIME, Am. Inst. of Mining, Metall., and Pet. Eng., Denver, Colo., 9 –12 Oct. 1977.

Cosentino, P., A. Cimino, and A. M. Riggio, Time variations of the resistivity in a layered structure with unconfined aquifer, *Geoexploration*, *17*, 11–17, 1979.

Daily, W., and A. Ramirez, Evaluation of electromagnetic tomography to map in situ water in heated welded tuff, *Water Resour. Res.*, *25*, 1083–1096, 1989.

Davis, J. L., and A. P. Annam, Ground penetrating radar for high resolution mapping of soil and rock stratigraphy, *Geophys. Prospect.*, *37*, 531–551, 1989.

Dean, T. J., J. P. Bell, and A. J. B. Baty, Soil moisture measurement by an improved capacitance technique, part I, Sensor design and performance, *J. Hydrol.*, *93*, 67–68, 1987.

Eppstein, M. J., and D. E. Dougherty, Efficient three-dimensional data inversion: Soil characterization and moisture monitoring from cross-well ground-penetrating radar at a Vermont test site, *Water Resour. Res.*, *34*, 1889–1900, 1998.

Flury, M., H. Fluhler, W. A. Jury, and J. Leuenberger, Susceptibility of soils to preferential flow of water: A field study, *Water Resour. Res.*, *30*, 1945–1954, 1994.

Gardner, W., and D. Kirkham, Determination of soil moisture by neutron scattering, *Soil Sci.*, *73*, 391–401, 1952.

Goldman, M., B. Rabinovich, M. Rabinovich, D. Gilad, I. Gev, and M. Schirov, Application of the integrated NMR-TDEM method in groundwater exploration in Israel, *J. Appl. Geophys.*, *31*, 27–52, 1994.

Griffiths, D. H., and R. D. Barker, Two-dimensional resistivity imaging and modeling in areas of complex geology, *J. Appl. Geophys.*, *29*, 211–226, 1993.

Griffiths, D. H., and J. Turnbull, A multi-electrode array for resistivity surveying, *First Break*, *3*, 16–20, 1985.

Griffiths, D. H., J. Turnbull, and A. I. Olayinka, Two-dimensional resistivity mapping with a computer controlled array, *First Break*, *8*, 121–129, 1990.

Hagrey, S. A., and J. Michaelsen, Resistivity and percolation study of preferential flow in vadose zone at Bokhorst, Germany, *Geophysics*, *64*, 746–753, 1999.

Heimovaara, T. J., and W. Bouten, A computer-controlled 36-channel time domain reflectometry system for monitoring soil water contents, *Water Resour. Res.*, *26*, 2311–2316, 1990.

Herkelrath, W. N., S. P. Hamburg, and F. Murphy, Automatic, real-time monitoring of soil moisture in a remote field area with time domain reflectometry, *Water Resour. Res.*, *27*, 857–864, 1991.

Hubbard, S. S., Y. Rubin, and E. Majer, Ground-penetrating radar assisted saturation and permeability estimation in bimodal systems, *Water Resour. Res.*, *33*, 971–990, 1997.

Hubbard, S. S., K. Grote, and Y. Rubin, Mapping the volumetric soil water content of a California vineyard using high-frequency GPR ground wave data, *Leading Edge*, *21*, 552–559, 2002.

Huisman, J. A., C. Sperl, W. Bouten, and J. M. Verstraten, Soil water content measurements at different scales: Accuracy of time domain reflectometry and ground-penetrating radar, *J. Hydrol.*, *245*, 48–58, 2001.

Iliceto, V., Contribution à la prospection géophysique des sites archéologiques, Ph.D. thesis, Univ. de Paris, Paris, 1969.

Isambert, M., and O. Duval, Notice explicative de la carte pédologique de Villamblain (Beauce) au 1/10000ème, contrat de recherche site expérimental de Villamblain, rapport période 1991–1992, 38 pp., Serv. d'Etude des Sols et de la Carte Pédol. de France, Ardon, 1992.

Kung, K. J. S., Preferential flow in a sandy vadose zone: I Field observation, *Geoderma*, *46*, 51–58, 1990a.

Kung, K. J. S., Preferential flow in a sandy vadose zone: II Mechanism and implication, *Geoderma*, *46*, 59–71, 1990b.

Loke, M. H., and R. D. Barker, Rapid least-squares inversion of apparent resistivity pseudosections using a quasi-Newton method, *Geophy. Prospect.*, *44*, 131–152, 1996.

Michot, D., A. Dorigny, and Y. Benderitter, Mise en évidence par résistivité électrique des écoulements préférentiels et de l'assèchement par le maïs d'un Calcisol de Beauce irrigué, *C. R. Acad. Sc. Paris*, Série Iia, *332*, 29–36, 2001.

Mualem, Y., and S. P. Friedman, Theoretical prediction of electrical conductivity in saturated and unsaturated soil, *Water Resour. Res.*, *27*, 2771–2777, 1991.

Nicoullaud, B., R. Darthout, and O. Duval, Etude de l'enracinement du blé tendre d'hiver et du maïs dans les sols argilo-limoneux de Petite Beauce, *Etude et Gestion des Sols*, *2*, 183–200, 1995.

Nicoullaud, B., O. Duval, M. Eimberck, A. Dorigny, and M. Isambert, Cartographie pédologique, Aspects sur le terrain, Livret guide, Organisation de la couverture pédologique et modélisation des processus spatiaux, Journées de formation jeunes chercheurs, 26–30/05/1997, Orléans. INRA, Département de Science du Sol., 34 pp., 1997.

Panissod, C., D. Michot, Y. Benderitter, and A. Tabbagh, On the effectiveness of 2D electrical inversion results: An agricultural case study, *Geophysical Prospecting*, *49*, 570–576, 2001.

Park, S., Fluid migration in the vadose zone from 3-D inversion of resistivity monitoring data, *Geophysics*, *63*, 41–51, 1998.

Parkin, G., D. Redman, P. V. Bertoldi, and Z. Zhang, Measurement of soil water content below a wastewater trench using ground-penetrating radar, *Water Resour. Res.*, *36*, 2147–2154, 2000.

Revil, A., L. M. Cathles III, S. Losh, and J. A. Nunn, Electrical conductivity in shaly sands with geophysical applications, *J. of Geophysical. Research.*, *103*, 23,925–23,936, 1998.

Ritsema, C. J., and L. W. Dekker, How water moves in a water repellent sandy soil, 2, Dynamics of fingered flow, *Water Resour. Res.*, *30*, 2519–2531, 1994.

Ritsema, C. J., L. W. Dekker, J. M. H. Hendrickx, and W. Hamminga, Preferential flow mechanism in water repellent sandy soil, *Water Resour. Res.*, *29*, 2183–2193, 1993.

Robert, P. C., Precision agriculture: Research needs and status in the USA, 2nd European Conference on Precision Agriculture, Odense, Denmark, 11–15 July, 19–34,1999.

Rothe, A., W. Weis, K. Kreutzer, D. Matthies, U. Hess, and B. Ansorge, Changes in soil structure caused by the installation of time domain reflectometry probes and their influence on the measurement of soil moisture, *Water Resour. Res.*, *33*, 1585–1593, 1997.

Scanlon, B. R., and R. S. Goldsmith, Field study of spatial variability in unsaturated flow beneath and adjacent to playas, *Water Resour. Res.*, *33*, 2239–2252, 1997.

Schnebelen, N., E. Ledoux, A. Bruand, and G. Creuzot, Stratification hydrogéochimique et écoulements verticaux dans l'aquifère des Calcaires de Beauce (France): Un système anthropisé à forte variabilité spatiale et temporelle, *C. R. Acad. Sci. Paris, Ser. IIa*, *329*, 421–428, 1999.

Sheets, K. R., and J. M. H. Hendrickx, Non-invasive soil water content measurement using electromagnetic induction, *Water Resour. Res.*, *31*, 2401–2409, 1995.

Shima, H., Two dimensional automatic resistivity inversion technique using alpha centers, *Geophysics*, *55*, 682–694, 1990.

Tabbagh, A., Y. Benderitter, D. Michot, and C. Panissod, Measurement of variations in soil electrical resistivity for assessing the volume affected by plant water uptake, *Eur. J. Environ. Eng. Geophys.*, *7*, 229–237, 2002.

Tardieu, F., and H. Manichon, I-Etat structural, enracinement et alimentation hydrique du maïs, II-Croissance et disposition spatiale du système racinaire, *Agronomie*, *7*, 201–211, 1987.

Topp, G. C. and J. L. Davis, Time-domain reflectometry (TDR) and its application to irrigation scheduling, in *Advances in Irrigation*, vol. 3, edited by D. Hillel, pp. 107–127, Academic, San Diego, Calif., 1985.

Topp, G. C., J. L. Davis, and A. P. Annan, Electromagnetic determination of soil water content, Measurements in coaxial transmission lines, *Water Resour. Res.*, *16*, 574–582, 1980.

Ward, S. H., Resistivity and induced polarisation methods, in *Geotechnical and Environmental Geophysics*, vol. 1, edited by S. H. Ward, pp. 147–189, Soc. of Exp. Geophys., Tulsa, Okla., 1990.

Waxman, M. H., and L. J. M. Smits, Electrical conductivities in oil-bearing shaly sand, *Soc. Pet. Eng. J.*, *8*, 107–122, 1968.

Weiler, K. W., T. S. Steenhuis, J. Boll, and K. J. S. Kung, Comparison of ground penetrating radar and time domain reflectometry as soil water sensors, *Soil Sci. Soc. Am. J.*, *62*, 1237–1239, 1998.

White, P. A., Electrode arrays for measuring groundwater flow direction and velocity, *Geophysics*, *59*, 192–201, 1994.

Worthington, P. F., The evolution of shaly sand concepts in reservoir evaluation, *Log Anal.*, *26*, 23–40, 1985.

Wyllie, M. R. J., and P. F. Southwick, An experimental investigation of the S. P. and resistivity phenomena in dirty sands, *J. Pet. Technol.*, *6*, 44–57, 1954.

Zhang, J., R. L. Mackie, and T. R. Madden, 3-D resistivity forward modeling and inversion using conjugate gradients, *Geophysics*, *60*, 1313–1325, 1995.

Zhou, Q. Y., J. Shimada, and A. Sato, Three-dimensional spatial and temporal monitoring of soil water content using electrical resistivity tomography, *Water Resour. Res.*, *37*, 273–285, 2001.

Y. Benderitter and A. Tabbagh, UMR 7619 "Sisyphe", UMPC, CNRS, case 105, 4 Place Jussieu, 75252 Paris Cedex 05, France.

A. Dorigny, D. King, D. Michot, and B. Nicoullaud, Institut National de la Recherche Agronomique Orléans, Unité de Science du Sol, BP 20619, 45166 Olivet Cedex, France. (didier.michot@orleans.inra.fr)